ATMOSPHERIC BOUNDARY LAYER CHARACTERISTICS USING MONOSTATIC SODAR

A Dissertation submitted in fulfillment of the requirements for the Degree

of

MASTER OF ENGINEERING

in

Electronic Instrumentation & Control Engineering

Submitted by

Nishant Kumar
Reg No. - 801351015

Under the Guidance of

Dr. Kirti Soni
Scientist, AUV Standards
CSIR-National Physical Laboratory
New Delhi

Dr. Ravinder Agarwal
Professor, EIED
Thapar University
Patiala

2015

Electrical and Instrumentation Engineering Department
Thapar University, Patiala
(Declared as Deemed-to-be-University u/s 3 of the UGC Act., 1956)
Post Bag No. 32, Patiala – 147004
Punjab (India)

सी.एस.आई.आर.-राष्ट्रीय भौतिक प्रयोगशाला
(वैज्ञानिक तथा औद्योगिक अनुसंधान परिषद्)
CSIR-NATIONAL PHYSICAL LABORATORY
(Council of Scientific & Industrial Research)
डा० के. एस. कृष्णन् मार्ग, नई दिल्ली-110012
Dr. K.S. Krishnan Marg, New Delhi-110012

CERTIFICATE

This is to certify that **NISHANT KUMAR**, M.E. (Electronic Instrumentation and Control Engineering) student of Thapar University, Patiala has completed the dissertation entitled "**Atmospheric Boundary Layer Characteristics Using Monostatic SODAR**" under the supervision of **Dr. KIRTI SONI**, Scientist, Acoustics, Ultrasonics and Vibration (AUV) Standards at CSIR-NPL, New Delhi. This project has been carried out during the period of 2nd January 2015 to 30th June 2015 in AUV Standards.

During the tenure of his project training, he displayed high professional and discipline towards his job. He has shown full dedication and commitment during his training.

I wish him all the best in his future endeavors.

Dr. KirtiSoni
Scientist, AUV Standards
CSIR-NPL, New Delhi

Dr. Mahavir Singh
Head, AUV Standards
CSIR-NPL, New Delhi

Dr. Rajeev Chopra
Head, HRD Group
CSIR-NPL, New Delhi

Fax / फैक्स : 91-11-45609310
Director Office : 45609201 / 45609301
COA's Office : 45609203
COS&P's Office : 45608367
SPO's Office : 45609326
ई-मेल : root@nplindia.org
E-mail : root@nplindia.org
वेबसाईट/Website : www.nplindia.org

NATIONAL PHYSICAL LABORATORY (HRD GROUP) Endorsement No. 2386/65/14

DECLARATION

I hereby certify that the work which is presented in dissertation entitled, "**Atmospheric Boundary Layer Characteristics Using Monostatic SODAR**", in partial fulfillment of the requirements for the award of the degree of Master of Engineering in Electronic Instrumentation and Control Engineering, submitted to Electrical & Instrumentation Engineering Department of Thapar University, Patiala is as authentic record of my own work carried under the supervision of Dr. Ravinder Agarwal. It refers others researcher's work which is duly listed in the reference section. The matter contained in this dissertation has not been submitted, neither in part nor in full to any other degree to any other university or institute except as reported in the text and references.

Place: Patiala
Date: 13/07/2015

Nishant Kumar
(Nishant Kumar)
Roll No.: 801351015

It is certified that the above statement made by the student is correct to the best of my knowledge and belief.

Date: 13/07/2015

(Dr. Ravinder Agarwal)
Professor
Electrical & Instrumentation Engineering Department
Thapar University, Patiala

Countersigned by:

Dr. Ravinder Agarwal
Head
Electrical & Instrumentation Engineering Department
Thapar University, Patiala

Dr. S.S. Bhatia
Dean (Academic Affairs)
Thapar University, Patiala

ACKNOWLEDGEMENT

I am grateful to my M.E. thesis supervisor **Dr. Ravinder Agarwal, Professor**, Department of Electrical and Instrumentation Engineering, Thapar University, Patiala whose help, stimulating suggestions and encouragement helped me in all the time of research for and writing of this thesis. I could not have imagined having a better advisor and mentor for my M.E. study.

I express my sincere regard from the bottom of my heart to my Cosupervisor **Dr. Kirti Soni,** Scientist, CSIR-NPL, New Delhi for her valuable suggestions and discussions.

I am also highly thankful to **Dr. Ravinder Agarwal,** Head, **Mr. Nirbhowjap Singh**, P.G. coordinator of M.E. (EIC), and my venerable teachers, Department of Electrical and Instrumentation Engineering, Thapar University, Patiala for their invaluable suggestions and caring concern at every stage during the entire stretch of studies.

I am deeply indebted to **Dr. Mahavir Singh**, Head, AUV Standards, CSIR-NPL, New Delhi for his dynamic support, keen interest and special attention during the entire stretch of research pursuit. My heartiest thanks are due to **Mr. Gurbir Singh, Mr. Naveen Garg and Dr. Kulwinder Singh Parmar** for all help rendered to me besides taking personal pains to see the completion of my research. I am also highly thanking to **Dr. P.K. Dubey, Dr. Y.K. Yadav, Ms. Reeta Gupta** and other technical staff of AUV Standards, CSIR-NPL, New Delhi for their personal support and constant encouragement. I am also thanking to **Dr. A. K. Upadhayaya**, Scientist, RASD, CSIR-NPL, New Delhi for their personal support.

I am immensely thankful to **Dr. D. Saha**, Scientist, Central Pollution Control Broad, New Delhi for reviewing and assessing the progress of my research work and also for their valuable suggestions to augment the quality of my work.

I feel immense pleasure in expressing my regard, sincere appreciation and deep sense of gratitude to my Uncle **Sh. Shatrughan Prasad** (Advocate, Civil Court, Patna City), I am sure, without his support, and this would have never been a reality in my life.

Finally, I express my deepest feeling of gratitude and I pay my best regards to my parents who provided the best for me in my life.

I express my sincere gratitude to my friend **Ashutosh Sharma** for their generous help and continuous support.

Thank you all for your insights, guidance and support.

Nishant Kumar

(Nishant Kumar)

TABLE OF CONTENTS

LIST OF TABLES

LIST OF FIGURES

NOMENCLATURE

Main symbols and notations used in this study are listed below. Sometimes a symbol may have alternate meaning but in such a case; the context is sufficient to avoid confusion.

CSIR	Council of Scientific & Industrial Research
NPL	National Physical Laboratory
SODAR	Sonic Detection and Ranging
PBL	Planetary Boundary Layer
ABL	Atmospheric Boundary Layer
CBL	Convective boundary layer
ANN	Artificial neural network
FIS	Fuzzy inference system
ANFIS	Adaptive neuro-fuzzy interface system

ABSTRACT

The variability of atmospheric boundary layer along with meteorological parameters have been investigated. Two sources of data have been used in the present work: SODAR (Sound wave detection and ranging) and automatic weather station for the period from December 2013-November 2014. A LabVIEW based program has been developed to plot the stability class from A to F directly from mixing height data. Based on SODAR echograms and mixing height; temporal and seasonal variability of stability classes has been evaluated. Impact of meteorological parameters, i.e., wind speed, temperature and relative humidity on mixing height during different seasons have also been studied. A new method for prediction of ventilation coefficient is developed. In this study, wavelet, artificial neural network and fuzzy models in conjunction are utilized for developing a new model for prediction of ventilation coefficient. These studies shall be indispensable for the Air pollution management.

OBJECTIVES OF THE PRESENT STUDY

1. Study of annual and seasonal fluctuation of atmospheric boundary layer along with meteorological parameter.
2. Development of LabVIEW based program for the analysis and classification of stability class.
3. Study of stability class and its variability in different seasons and in different weather condition.
4. Development of wavelet-Neuro-fuzzy model for the prediction of ventilation coefficient.

CHAPTER 1

INTRODUCTION OF ATMOSPHERIC

1.1. Introduction

The present atmosphere of the Earth is probably not its unique atmosphere. Our current atmosphere is what chemists would call an oxidizing atmosphere, while the original atmosphere was what chemists would call a reducing atmosphere. In particular, it probably did not carry oxygen.

1.2. Composition of the Atmosphere

The unique atmosphere may have been similar to the composition of the solar nebula and close to the present composition of the Gas Giant planets, though this depends on the particulars of how the planets condensed from the solar nebula. That atmosphere was lost in distance, and substituted by compounds out gassed from the crust or (in some more recent theories) a lot of the atmosphere may have come in its place from the impacts of comets and other planetesimals rich in volatile materials.

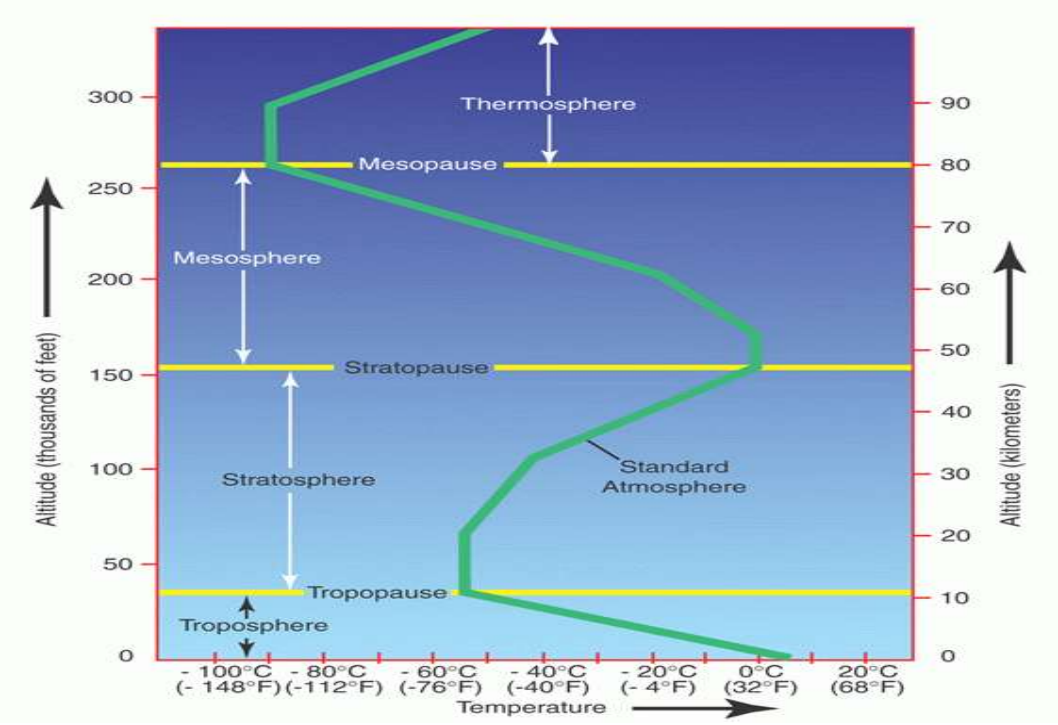

Figure 1.1. Vertical temperature profile in the atmosphere

The oxygen, so characteristic of our atmosphere was almost all produced by plants (cyanobacteria or, more colloquially, blue-green algae). Thus, the present composition of the atmosphere is 79% nitrogen, 20% oxygen, and 1% other gases.

1.3. Layers of the Atmosphere

The atmosphere of the Earth may be divided into several distinct layers, as the following figure 1.2 indicates.

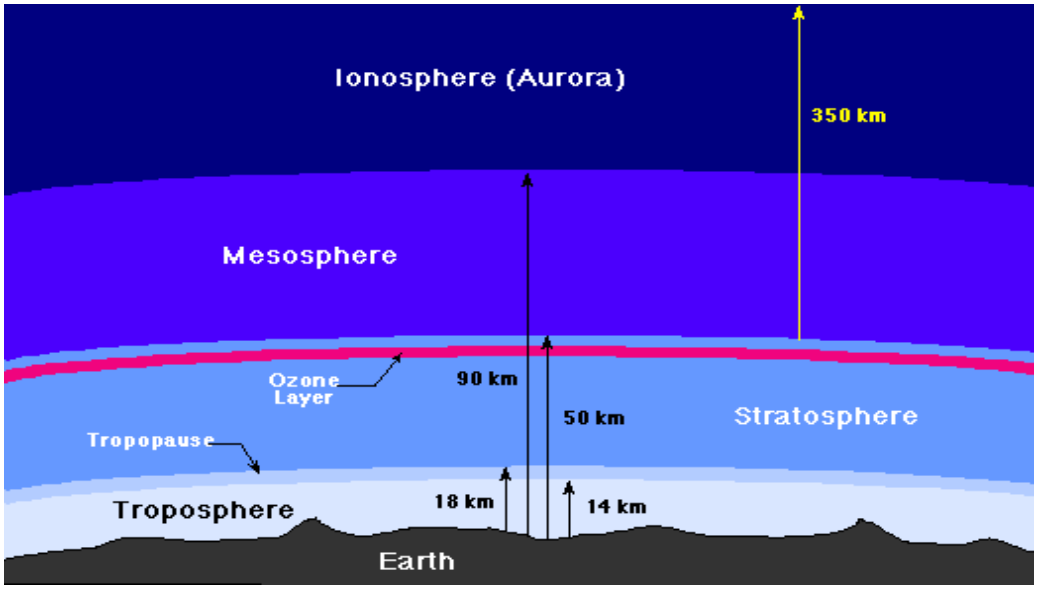

Figure 1.2. Different layers of atmosphere

1.3.1. Troposphere

The troposphere is where all weather takes place; it is the region of ascending and falling packets of air. The air pressure at the height of the troposphere is only 10% of that at sea level (0.1 atmospheres). There is a thin buffer zone between the troposphere and the next layer called the tropopause (where temperature increases to decrease).

Troposphere literally means the "region of mixing". The median elevation of this lowermost layer of the atmosphere up to 10 to 16 Km (10 km in the Polar region and 16 km in the tropical region). The lowermost portion of the troposphere is further split into 3 sublayers:

1. The Planetary Boundary Layer (PBL)
2. The Surface Boundary Layer
3. The Laminar Layer

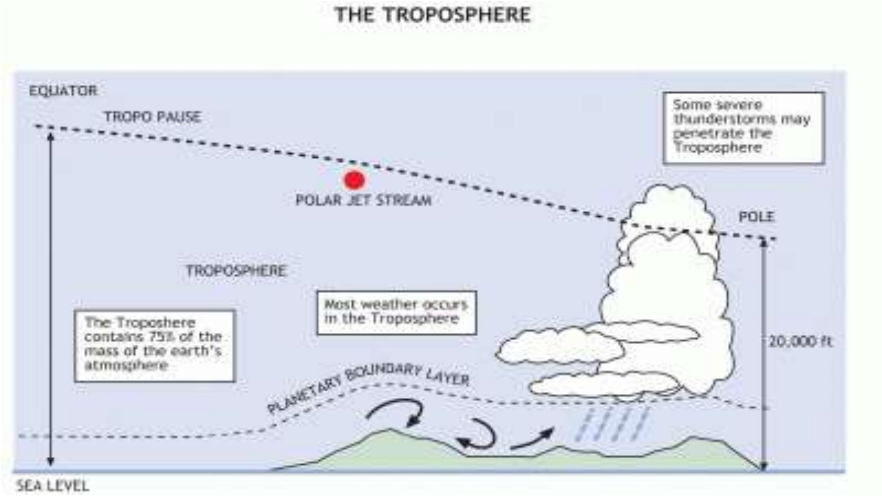

Figure 1.3. Planetary boundary layer

1.3.2. Stratosphere

Above the troposphere is the stratosphere, where air current is generally horizontal. The thin ozone layer in the upper stratosphere has a high concentration of ozone, a particularly reactive form of O. This layer is chiefly responsible for absorbing the UV irradiation from the Sun due to this temperature that increases with elevation.

1.3.3. Mesosphere

Above the stratosphere is the mesosphere, this area is characterized by rapid vertical mixing because of penetration of ultraviolet radiation.

1.3.4. Thermosphere

Above the mesopause, this area is likewise recognized as the ionosphere (or thermosphere), where many particles are ionized. In this part, the temperature increases to reach highest values that are extremely dependent on input solar energy.

1.4. Planetary Boundary layer

In 1904 the concept of a boundary layer, where a moving fluid meets a solid boundary, was first reported by Ludwig Prandtl. He indicated that the stream could be separate into two areas, the majority of the flow where viscosity could be neglected (which was what most of the previous work had acquired), and the boundary layer around the surface of an object where viscosity was important, and where the tangential velocity of the flow to the surface fell rapidly to zero. Planetary

boundary layer (PBL), also called an atmospheric boundary layer, the part of the lower troposphere where the Earth's surface strongly influences temperature, wet, and wind through the turbulent transport of air volume. The thickness (depth) of the PBL is not constant, normally about 1-1.5 kilometer deep, but in mid-latitudes can vary from 100 m to 3 kilometer. At night and in the cool season the PBL tends to be lower in thickness while during the day and in the warm season it tends to cause a higher thickness. The two reasons for this are the wind speed and thickness of the air as a function of temperature, temperatures vary diurnally, unlike the free atmosphere above. Stronger wind speeds allow for more convective mixing. This convective mixing will cause the PBL to expand. At nighttime, the PBL contracts due to a reduction of rising thermals from the airfoil, the surface influences the ABL by friction and by heat fluxes at the land. Stale air is denser than warm air; therefore the PBL will tend to be shallower in the cool time of year. Thus, it is necessary for uninterrupted monitoring of PBL; because

1. Pollution in big city continues to increase and this pollution are dispersing in PBL
2. Humans are living in the boundary layer
3. Local forecasts
4. Impression on the residue of the air
5. Boundary-layer clouds are really important for climate, Boundary layer clouds: predominantly fair-weather cumulus, stratocumulus and fog.

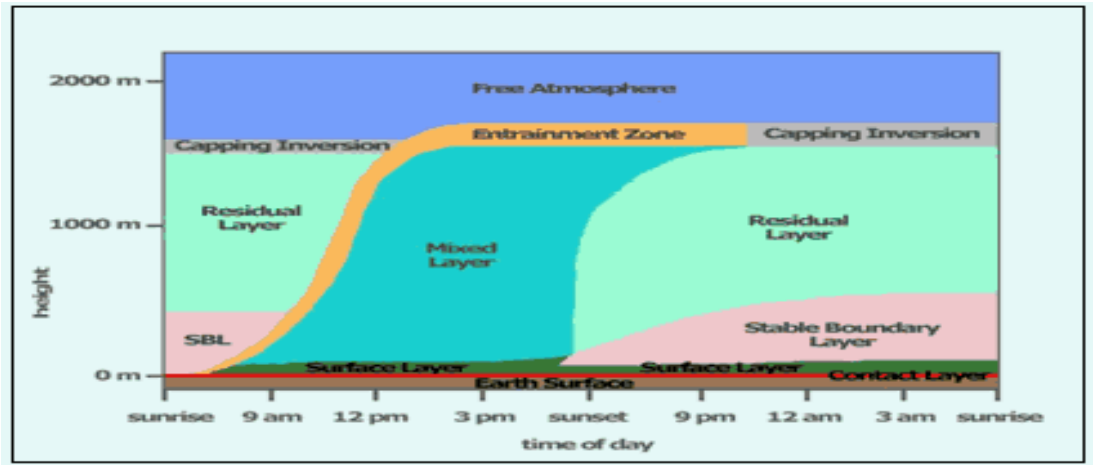

Figure 1.4. Temporal variation of PBL

Figure 1.4. Illustrates a typical daytime evolution of the atmospheric boundary layer over land. The solar heating causes thermal plumes to rise, transporting moisture, heat and aerosols. The plumes rise and expand adiabatically until a thermodynamic equilibrium is reached at the top of

the atmospheric boundary layer. The moisture removed from the thermal plumes forms convective clouds.

Drier air from the free atmosphere penetrates down, replacing rising air parcels. The region of the troposphere between the highest thermal plume tops and deepest parts of the sinking free air is called the entertainment zone. The convective air motions generate intense turbulent mixing. This tends to get a mixed layer, which has potential temperature and humidity nearly constant with altitude. When buoyant turbulence generation dominates the mixed layer, it is sent for a convective boundary layer (CBL). The lowest region of the ABL is called the surface layer. In windy conditions, the surface layer is characterized by a strong wind shear caused by rubbing.

The boundary layer from sunset to sunrise is called the nocturnal boundary layer. It is frequently qualified by a stable layer, which works when the solar heating ends and the radiative cooling and surface friction stabilize the lowest percentage of the ABL. Above that, the remnants of the daytime CBL form a residual layer. The nocturnal boundary layer may also be convective when cold air advects over a warm surface.

The mixing height is the height of the top of the surface based layer in which vertical mixing of pollutants is relatively vigorous and lapse rate is approximately dry-adiabatic. It passes on the top of the atmospheric layer up to which pollutants get mixed vertically i.e. height of the atmosphere above the earth's surface to which released air pollutants will extend primarily through the action of atmospheric turbulence. Vertical mixing can be determined by SODAR.

Atmospheric layer in which temperature increases with height is known as inversion. The inversion may be ground based or elevated depending on the meteorological conditions.

1.4.1. Temperature behavior

The dry adiabatic lapse rate of temperature with height is round 9.8^0C/km. Under certain conditions, the lapse rate even changes sign (inversions). Depending upon the nature of the temperature gradient, two states of the atmosphere, static stability and instability, exist in nature.

1.4.2. Wind profile

As we go up in the atmosphere from the surface of the earth, the wind velocity increases. The increase of velocity with height up to 300-400 m is very regular. However, it varies irregularly at higher heights. The velocity of the surface winds has a well-defined daily period on land. The

velocity is least in the morning hours and is the largest in the afternoon. The change is larger on clear days than on cloudy days, is most pronounced in summer and is the least in winter.

1.4.3. Variation of humidity

The humidity variations contribute by far the most important variations in the lower atmosphere. As a result of evaporation, water vapor rises from the earth's surface and tends to diffuse through the atmosphere. Under calm conditions, diffusion is very slow. It increases, by a factor as large as 1000 under turbulent atmospheric conditions. Percentage humidity, therefore, varies only a few in a turbulent medium, but may have a very steep gradient with respect to height in a stable region. Humidity follows a diurnal variation under normal conditions. It is seen that humidity starts decreasing with sunrise, attains a minimum during the day, increases after sunset in the evening and attains a maximum in the early morning hours.

1.5. Monitoring Techniques

There are various techniques, with relative merits, in use to probe the lower atmosphere. These techniques are broadly classified into the following two categories:

1. Direct or in-situ measurement techniques.
2. Remote sensing techniques.

There are several methods to find out mixing height such as using temperature profiles measured by radiosonde, tethered balloon or instrumented tower and by remote sensing with RASS, LIDAR or SODAR.

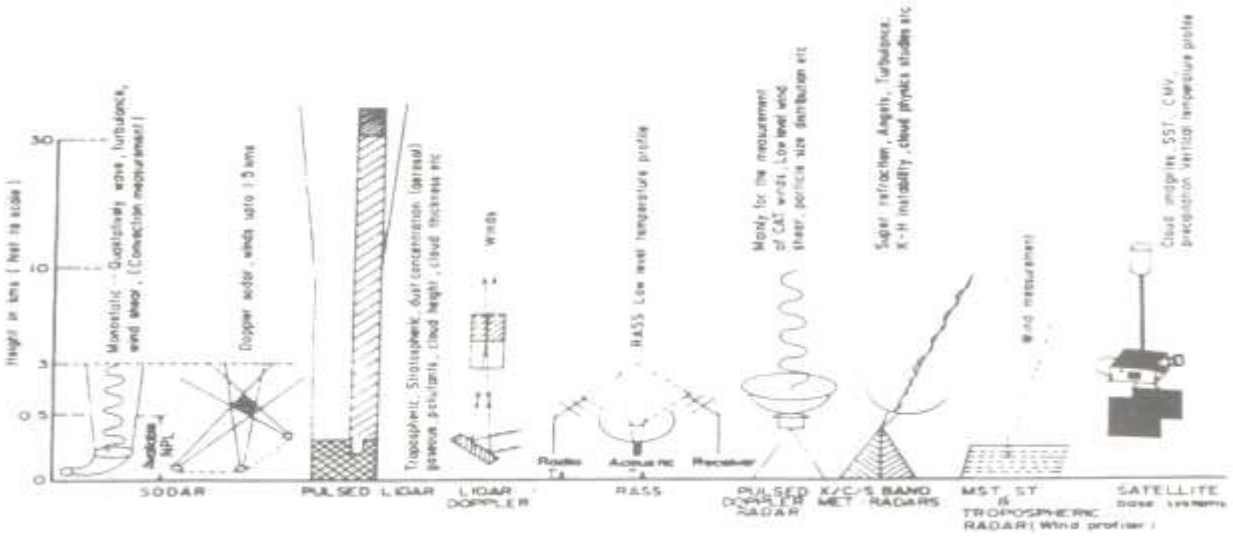

Figure 1.5. Comparison of various techniques

Table 1.1 Comparative capabilities of various In-situ techniques

S.No.	Parameters		Radiosonde	Tethered balloon	Instrumented Tower	Refractometer
1	Typical operating range	Max.	18 Km.	1 Km.	300 m	10 Km
		Min.	150 m	10 m	3 m	Ground
2	Range Resolution		60 m	10 m	3 m	10 m
3	Advantages		Long range	Higher resolution	Higher resolution and continuity of data	Greater accuracy and fast response time
4	Major limitations		Poor resolution, discontinuity in data	Low max. range, discontinuity in data	Very low max. range	Cost effective device
5	Nature of tracers		Temperature, humidity, and wind	Temperature, humidity and wind	Temperature and wind	Refractivity
6	Accuracy in measurement		$\pm 0.5^0$C ± 1 m bar Minimum of humidity 15%	0.5^0C 1 m bar	0.1^0C 0.5 m/sec	± 1N units

Table 1.2 comparative capabilities of various remote sensing techniques

S. No.	Parameters		RADAR		SODAR		LIDAR	RASS	Satellite Beacon
			Pulsed	**FM-CW**	**Monostatic**	**Bistatic**			
1	Typical operating range	Max.	50 Km.	1 Km.	3 Km.	3 Km.	3 Km.	3 Km.	Integrated range
		Min.	300 m	30 m	30 m	10 m	10 m	10 m	
2	Spatial resolute-ion	Range	100 m	2 m	10 m	50 m	3 m	30 m	----
		Angular beam width	10	30	100	---	1 mm	---	20
3	Typical time between successive measurements		1 sec.		10 sec		10-2 sec.	10 sec.	---
4	Typical wavelength/ frequency		5-10 cm/GHz		1000-5000 Hz.		6000-7000 A^0	80-100 Hz/36.8 MHz	40 MHz to 300 GHz
5	Scale size		Mesoscale		Small Scale		Micro scale	Small scale	Small scale
6	Nature of tracer		Precipitation Cn, insects etc		C_T	C_T, C_V		C_n	C_n^2
7	Patterns		Radial velocity and atmospheri c structure	Radial velocity and atmospher ic structure	Radial velocity and thermal structures	Total wind vector and thermal structures	Radial velocity Aerosol distribution	Temperature profile	Refractivity
8	Major advantages		Lang range high information rate, identificati on of layers and waves	High resolution lower mini-mum range	Abundance of natural tracers low cost, high scattering cross section	Natural tracers abundant, higher sensitivity in forward direction	High resolution high data rate	Continuous temperature measurement	Potential technique in case of geostationary satellite
9	Major limitations		Natural tracers rarely sufficient poor spatial resolution high min. range	Low range	Low range	Low range	Alternation due to cloud and haze. Possible radiation hazard	Higher cost	Limited geometry, Availability of satellite

1.6. SODAR as a Monitoring Technique

SODAR is one of the best remote sensing techniques which is internationally recognized and proven cost effective to provide continuous real time data of air pollution meteorological parameters such as mixing height / inversion height, ABL stability and wind profile. It is internationally recognized and recommended by EPA for air quality dispersion modelling in EIA. This technique is in use all over the world for various practical and ABL research applications. Occurrence of thermal convection, inversion, elevated inversion; advection, subsiding air mass, sudden gust, waves etc. are easily identified in SODAR records. SODAR provides useful information about evolution characteristics of coastal boundary layer phenomena (Sea/Land breeze/TIBL). Information can be used as an aid to assess/ understand signal performance of communication links in real time. During sunny weather, air closer to the Earth's surface becomes much warmer compared to the air aloft. Thus, it becomes lighter and moves up. On SODAR, this vertical movement in the form of thermal plumes has been observed (dense inverted cones). SODAR is one of the best techniques (acoustic remote sensing) to probe atmospheric boundary layer (ABL) in real space and time up-to the height of 3 km.

CHAPTER 2

SODAR AND METEOROLOGY TOWER

2.1 Introduction

The acoustic waves through used as early as 1874 by Tyndall and many others later on for studying the lower atmosphere, the potential use of these waves for monitoring the lower atmosphere was established by the development of a monostatic SODAR by McAllister in the year 1968. The SODAR technique has been lately adopted all over the globe (U.S.A., Australia, Japan, France, Germany, Canada and India). In India, work was taken up at the National Physical Laboratory, New Delhi on the 1972.

2.2. Principle of SODAR

Schematic for the principle of SODAR is shown in figure 2.1. This technique basically relies on transmitting a pulsed narrow beam of sound into the atmosphere where it encounters atmospheric inhomogeneities and suffers partial reflection. The scattered signals are received by the same transducer (monostatic) or by another transducer (bistatic). In either operational mode the delay time and intensity are measured with each echo scan in the form of intensity modulation on a sweep recorder of the PC, displaying height range (ordinate) versus time (abscissa) pictures called echograms. The acoustic echoes depicted on the echograms tend to be of two major types the inversion echoes and thermal echoes. Inversion echoes tend to be horizontal and continuous in time while thermal echoes appear as vertical intermitted spikes.

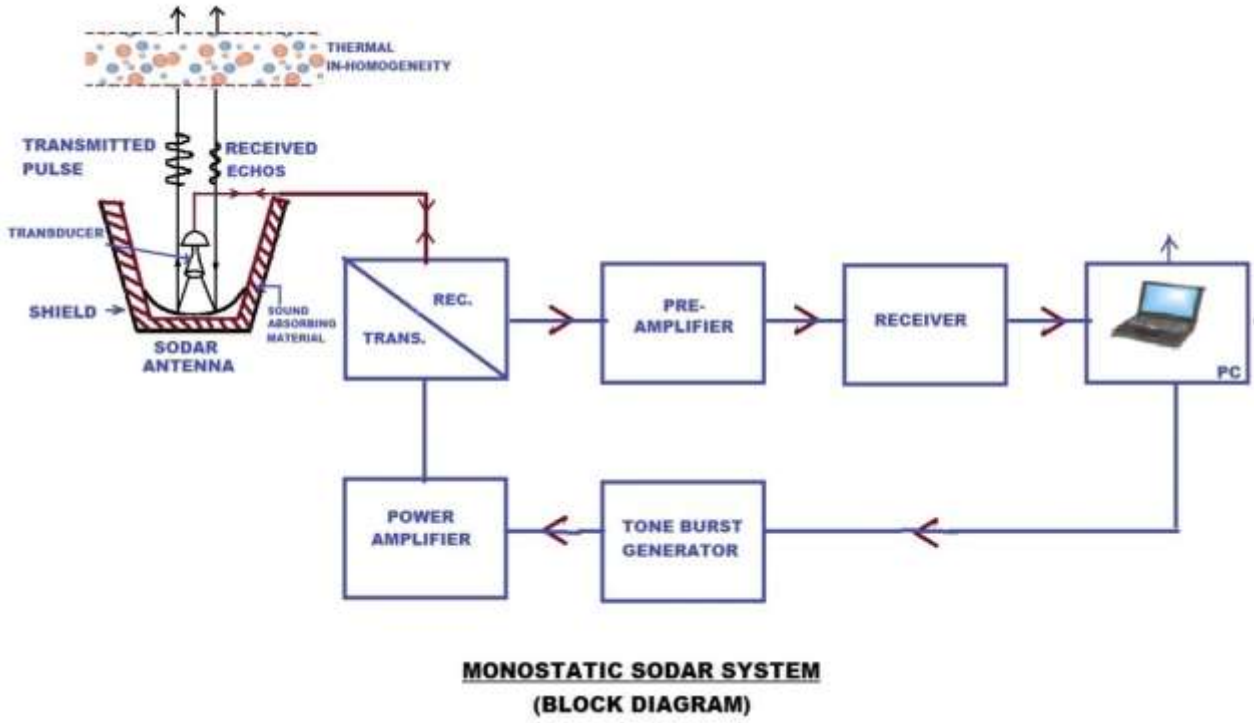

Figure 2.1. Block diagram of SODAR system

2.3. SODAR configuration

SODAR can be configured as single axis monostatic or bistatic and three axis system using an antenna depending upon the system configuration they may be used to sense one or more component of the vector wind as a function of height. These configurations are presented here.

2.3.1. Monostatic SODAR

The simplest system configuration is a vertically pointed single frequency monostatic system, as it is shown in figure 2.1. For wind measurements this system can also be controlled by tilting the parabolic dish at some prescribed angle. Because the vertical pointing system, is a special case ($\theta=\pi/2$) for tilted system, it is helpful to develop the SODAR equation for it and then substitute ($\theta=\pi/2$) for the vertical pointing configuration.

In SODAR system it is assumed that the thickness of the layer 'L' scattering the sound is much less than the SODAR pulse length i.e.

$$L \ll C\tau \qquad (2.1)$$

A monostatic SODAR is used to measure radial components of the wind velocity in the direction of the sound pulse with the help of the repeated equation

$$V=\lambda.\Delta f \qquad (2.2)$$

where V is Doppler velocity, Δf is Doppler frequency shift and λ is transmitted wavelength. Monostatic SODAR may be run in a vertical manner to assess the perpendicular portion of the wind velocity or tilted at an appropriate angle to measure the horizontal element of wind. The error in horizontal wind is in order of 0.5 m/s. In lodge to avoid these errors one may hold to take a longer pulse at the expense of range due to fading. Ace may as well take a narrower receiver bandwidth, however, trade off here is the need to sustain the required Doppler dynamic range, and the only option may be to use more samples in the norm.

2.3.2. Bi-static SODAR

Monostatic SODAR has a major application in thermal gradient detection and single axis Doppler measurements. The monostatic SODAR system, nevertheless, holds a major drawback in that their role may be limited for continuous wind profiling. Monostatic echoes (in theory) are solely the effect of temperature produced fluctuation in the sampling volume the return therefore can be marginal, discontinues and provides gaps in the wind data. In a neutral atmosphere, no data would be received by the scattering angle for by static SODARS is in the range for the value of θ is zero or $\pi/2$. There will be echoes from both temperature and velocity structure function.

Bistatic SODAR is a system in which all of the transmitting and receiving antennas are separated in space but are aimed at a common volume.

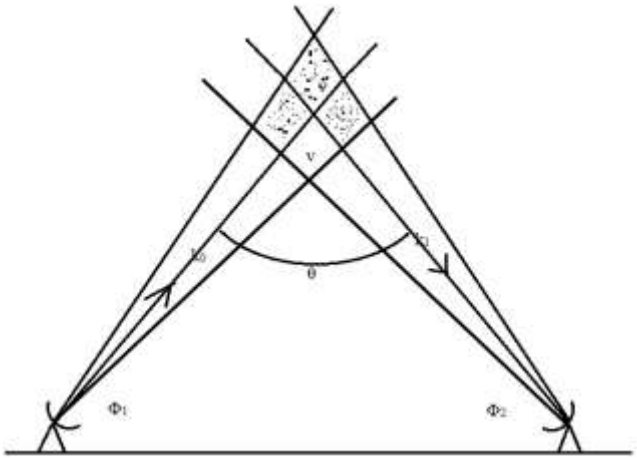

Figure 2.2. Bistatic SODAR

This configuration will yield a higher signal to noise ratio, since returns for both temperature and wind fluctuation contribute to the scattering. Wind profiles can be obtained by displacing the common volume up and downwards or by heading one of the beams mechanically or

electronically. Schematic representation of acoustic scattering in case of bistatic SODAR is illustrated in figure 2.2. in which acoustic beam is launched at an elevation angle $\varphi_0$and scatter wave received at angle $\varphi_1$with appear scattering angle $\theta = \varphi_0 + \varphi_1$defines the magnitude of the components of the mean wind in the initial and scattered direction by $m_0 = e_0 m$ and $m_1 = e_1 m$ where m is the vector with component $m_1 = w_i/co$

2.3.3. Three – axis Doppler SODAR

A three axis Doppler SODAR banks upon the well-known Doppler Effect according to which a propagating wave undergoes apparent change in frequency as a result of radial motion of the scattering. It functions like a monostatic SODAR but involves data processing for evaluation of change in frequency of transmitted signal due to wind. A knowledge of shift in frequency enables determination of wind speed while line integration of the measurement of the backscattered energy as a function of height gives facsimile representation of the ABL. Tone burst generated from the transmitter section is suitably amplified and transmitted into the atmosphere through three parabolic dish antenna in three different directions. Central antenna is located in the vertical direction, where as other two antennas are inclined to 300 with respect to the vertical antenna. The receiver section consists of preamplifier, narrow bandpass filter and a range amplifier. The filtered signal is passed on to the succeeding stages for further signal processing. The signal is processed for intensity display and wind profile evaluation.

Figure 2.3. Three axis Doppler SODAR

With measurements using three antennas pointing in three different directions, three radial velocity components are resolved to determine the actual wind components in a rectangular coordinate system.

2.4. Antenna

It must be weatherproof and most of SODAR differ in the antenna's approach. Alternatives:

Parabolic dish: The speaker is located at the focal point and commonly, it is shielded to reduce environmental interferences. When it is a multi-axes SODAR, one parabolic dish points vertically, and the other ones (generally two) are slightly inclined. All of them work at different frequencies and therefore, backscattered signals do not interfere with each other.

Array: Small high-frequency speakers (tweeters) are interconnected in a tray. By adding more tweeters, the power of the antenna can be increased and therefore it makes a smarter configuration. Furthermore, its main advantage is to steer a unique sound beam in any direction by using the phased-array technology and hence, a single antenna array can be adjusted to obtain data along multiple axes.

The main consideration is to protect the array speakers from water under rainy situations. Basically, there are two approaches:

1. Folded tweeters:
2. Reflector board to avoid pointing upward.

2.5. Theoretical Considerations

SODAR technique is based on the theoretical analysis of acoustic wave scattering due to fluctuation in atmospheric acoustic refractive index due to temperature, wind or humidity. Propagating sound waves undergo changes in phase and amplitude on passing through regions of varying acoustic refractive index. The basic equation for the scattering of sound waves from the random fluctuation of atmospheric temperature and wind velocity within a turbulent region have been developed by Kallistratova (1961), Tatarskii (1961) and Monin (1962). For a Kolmogorov spectrum of turbulence in the inertial sub-range, the scattering cross section $\sigma(\theta)$ for acoustic waves has been demonstrated to be a function of scatter angle θ from the initial focal point of generation, propagating wavelength, turbulence parameters and is fed by,

$$\sigma(\theta) = 0.033\, k^{\frac{1}{3}} cos^2\theta \left[\frac{c_v^2}{c^2}\cos^2\frac{\theta}{2} + 0.13\,\frac{c_T^2}{T^2}\right] \qquad (2.3)$$

where σ (θ) is the scattering cross-section at an angle θ, c_v and c_T are the wind and temperature structure parameters defined respectively as

$$c_v^2 = \frac{\langle [u(\vec{x}) - u(\vec{x}+\vec{r})]^2 \rangle}{r^{\frac{2}{3}}} \qquad (2.4)$$

$$c_T^2 = \frac{\langle [T(\vec{x}) - T(\vec{x}+\vec{r})]^2 \rangle}{r^{\frac{2}{3}}} \qquad (2.5)$$

where measurements are made at two locations $\vec{x}$ and $\vec{x}+\vec{r}$ and $\langle\ \ \rangle$ indicates an ensemble average, normally approximated by a time average in practical applications.

The scattering equation shows that backscattering ($\theta=180^0$) is due to temperature inhomogeneities only while forward scattering takes into account both temperature and wind inhomogeneities. Moreover, scattering is a weak function of acoustic wavelength and there is no scattering at an angle of 90^0.

Little (1969) has shown that the backscattered power P_r is given by the basic expression:-

$$P_r = P_t\, \sigma(\theta)(c_\tau)\left(\frac{A_r L_a}{2R^2}\right) \qquad (2.6)$$

where P_t is the transmitted power, τ the pulse length (seconds).R the range (meters), A_r the effective receiving area, $L_a$the loss due to attenuation on the sound trip and σ (180^0) the backscattering cross-section at range R.

While incorporating antenna transducer efficiencies, Neff (1973) and later Kleppe (1989) transformed this equation as

$$P_r = P_t \eta_t \eta_r e^{-4\alpha} \sigma_0(R, f)\left(\frac{c_\tau}{2}\right)\left(\frac{A_r G}{R^2}\right) \qquad (2.7)$$

where P_r is received power (Watts), η_r is efficiency of conversion from received acoustical power to electrical power, $P_t\eta_t$ is radiated power where P_t is electrical power applied to the transducer and η_t is efficiency of conversion to radiated acoustic power

$e^{-4\alpha R}$ is round- trip loss of power resulting from attenuation by air where α is average attenuation (m^{-1}) to the scattering volume at range R(m), σ_0(R, f) is scattering cross-section per unit volume; i.e. fraction of incident power backscattered per unit distance into unit solid angle at frequency f, $c_\tau/2$ is maximum effective-scattering volume thickness where c is local speed of sound (m/s) & τ is pulse length (s)

$\left(\frac{A_r G}{R^2}\right)$ is solid angle subtended by the antenna aperture A(m^2) at range R (m) from the scattering volume, modified by an effective-aperture factor G, arising from antenna's directivity.

G is, in fact, the beam-shape compensation factor and is given by the expression:

$$G = \frac{G(o)\lambda^4 L^2(\theta_o)}{4\pi^2\theta_0^2 A^2} \quad (2.8)$$

where $L(\theta_0) = \left[1 - J_0^2\left(\frac{2\pi a\theta_0}{\lambda}\right) - J_1^2\left(\frac{2\pi a\theta_0}{\lambda}\right)\right]$

$$\theta_0 = \frac{\theta_{BW}}{2} = \frac{0.67\lambda}{D} = \frac{1.34\lambda}{a}$$

$$G(0) = \frac{4\pi A}{\lambda^2}$$

Here in a is the antenna radius at the aperture A, λ the transmitted wavelength and $J_n(x)$ the Bessel function of n^{th} order. In equation 6, θ_0 is one-half the total beam-width θ_{BW} and G(0) is the on-axis antenna gain. From equation 5, the intensity of the received acoustic signal, $I_s$can be expressed as

$$I_s = \frac{P_r}{\eta_r} A_r = [P_t \eta_t].[e^{-4\alpha R}]\left[\sigma_0(R,f)\left(\frac{c\tau}{2}\right)\left(\frac{G}{R^2}\right)\right] \quad (2.9)$$

Further that the total received noise intensity, I_n is the sum of the received acoustic noise level, N_a and the equivalent noise level, N_e of the system. Usually no>>N_e, and is regarded as an equivalent of the acoustic noise level, N_{am} multiplied by the directivity compensation factor for noises or side lobes, G_N and the diffraction attenuation effect, L_D i.e.,

$$I_n = G_N L_D N_{am} \quad (2.10)$$

The signal-to-noise ratio (SNR) is a critical factor in determining the delectability range of the SODAR echoes. The expression for SNR, given below forms an important base for design consideration of monostatic SODAR.

2.6. CSIR-NPL SODAR Characteristics

The setup of the Monostatic SODAR system working at CSIR-NPL is shown in figure 2.4 and figure 2.5. The whole system has been indigenously designed, developed and fabricated at CSIR-National Physical Laboratory, New Delhi. In the system the back scattering angle of the sound is 180^o, the pulses are received by the same antenna and it comes back from thermal inhomogeneities in the atmosphere. The SODAR system maps the height time function of the relative intensity of temperature eddies present in the lower atmosphere, which gives information of the of mixing height, inversion height, stability condition, time of onset and decay of thermal plumes, height of

fog layer, strength of turbulence etc. Along with data of acoustic sounding other meteorological information also will be required in air pollution studies.

The SODAR antenna is set up on the terrace of the 2nd floor of the main building of NPL, while the electronics and recording system is housed in a room located on the 1st floor of the main building. A parabolic dish of aperture 4 feet is used as the acoustic antenna. At the focus of the dish a transducer fitted with an exponential horn assembly is placed. The antenna dish is surrounded by the 7 foot high acoustic shield.

Top View

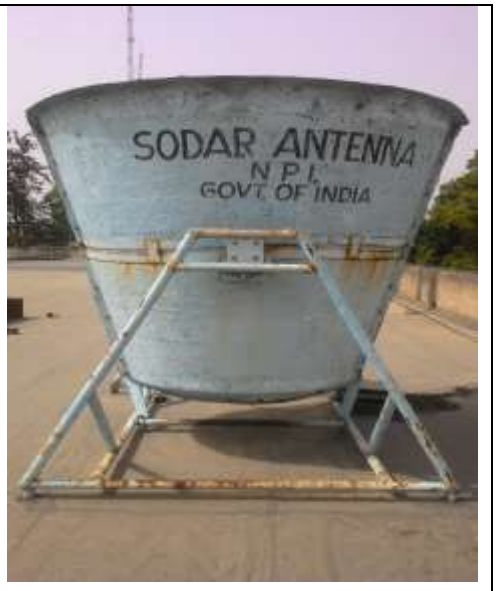

Side View

Figure 2.4. CSIR-NPL SODAR Antenna

SODAR is well recognized acoustic remote sensing technique that continues monitoring of atmospheric boundary layer (ABL) thermal structures in real time and space up to a height of (340m-3400m) depending on selectable range. Mixing height (MH) has been measured using CSIR-NPL monostatic SODAR system, which operated at many different frequencies according to requirement. The SODAR was operated at a frequency of 2.25 kHz with 50-350ms (selectable) pulse duration, a cycle time of (2-20) s (selectable) and electrical transmitting power of 50 W, acoustic power 10 W. Highly directional short bursts of sound energy are radiated into the atmosphere, which, after scattering from atmospheric fluctuations of eddy sizes within the inertial sub range (0.1–10 m), are received back by the receiving antenna. The signals are processed to produce an online display of the dynamics of ABL thermal structures. The echogram structural

details are further used to derive the mixing height of the ABL. The mixing height was obtained using the following empirical relationship given by (Singal, 1989).

$$y = 4.24*x+95 \quad (2.11)$$

where, y is the mixing height (m) for unstable atmospheric boundary layer, x is the depth of the SODAR measured thermal plumes (m).

The system operates at the fixed audio frequency of 2250 Hz. High power audible tone bursts of 100 ms duration are transmitted in every 6 seconds, which offer a probing range of about 3000 m of the lower atmospheric boundary layer. The operational frequency, duration of the tone burst and pulse repetition rate (determining the probing range) are selectable through a menu driven user friendly software for data acquisition.

Figure 2.5. Monostatic SODAR system at CSIR-NPL

Continuous hourly/monthly data are collected since the installation of SODAR at CSIR-NPL. The system specifications and the operational parameters are listed in Table 2.1.

Table 2.1.: Characteristics of CSIR-NPL (New Delhi) SODAR

Transmitted power (electrical)	90 Watts
Transmitted power (acoustical)	15 Watts
Pulse width	100 ms
Pulse repetition period	6 sec
Operational range	1000 m
Receiver bandwidth	50 Hz
Frequency of operation	2250 Hz
Acoustic velocity	340 m/s (average)
Receiver gain	80 dB
Transmit –receive antenna	Parabolic reflector dish surrounded by conical acoustic cuff
Receiver area	2.5 sq. m
Pre amplifier sensitivity	Fraction of a micro-Volt

2.7. CSIR-NPL Meteorological Tower

The setup of the meteorology tower is working in CSIR-NPL campus is shown in Figure 2.6. The whole system has been installed by Campbell scientific (Canada) Corp, USA. The meteorological tower is combination of atmospheric pressure sensor, temperature sensor, wind profile sensor, humidity sensor, solar radiation etc. This tower is used for continuous monitoring of meteorology condition.

Figure 2.6 Meteorology tower

2.7.1. Wind monitor

The wind monitor measures horizontal wind speed and direction. It is rugged and corrosion resistant, yet accurate and lightweight. The housing, nose cone, propeller and other components are injection molded U.V. stabilized plastic. Both the propeller and vertical shafts are stainless steel precision grade ball bearings.

Propeller rotation produces an AC sine wave signal with frequency proportional to wind speed. Internal circuitry converts the raw signal to 4 to 20mA current output over a specified wind speed range. The propeller consists of 18 cm diameter 4-blade helicoid polypropylene propeller, 29.4 cm air passage per revolution. The range of propeller is 0 to 60 m/s and gust survival 100 m/s.

Vane position is sensed by a 10K ohm precision conductive plastic potentiometer. This signal is also converted into 4 to 20 mA current output. The range of vane position is 360^0mechanical, 355^0 electrical.

2.7.2. Temperature and Humidity Probe

The HMP45C temperature and relative humidity probe contain a platinum resistance temperature detector (PRT) and a Vaisala HUMICAP 180 capacitive relative humidity sensor.

Table 2.2. Specifications Temperature and humidity probe

Parameter	**Value**
Operating temperature	-400C to +600C
Storage temperature	-400C to +800C
Probe length	25.4 cm
Probe body diameter	2.5 cm
Filter	0.2 µm Teflon membrane
Filter diameter	1.9 cm
Power consumption	< 4 mA @12 V
Supply voltage	7 to 35 VDC
Settling time	0.15 seconds
Temperature sensor	
Sensor	1000 ohm PRT, IEC 751 1/3 Class B
Temperature measurement range	-400 C to +600C
Temperature output signal range	0.008 to 1.0 V
Relative humidity sensor	
Sensor	HUMICAP 180
Relative humidity measurement range	0 to 100% non-condensing
RH output signal range	0.008 to 1 VDC
Response time	15 seconds with membrane filter

CHAPTER 3

SODAR STUDIES OF ATMOSPHERIC BOUNDARY LAYER AT NEW DELHI

A monostatic SODAR has been operated at the CSIR-NPL, New Delhi for the past several years to monitor the atmospheric boundary layer thermal structure upto a height of about 3000 m. During the course of observation various kinds of thermal and nocturnal structures have been observed. These structures of ABL have been studied to evolve a pattern recognition technique for identification and examination of the associated meteorological phenomenon. In this context, SODAR signatures of typical phenomena associated with topographical features and fair weather conditions viz. drainage wind, dust storm, monsoon boundary layer, fog conditions have been studied.

3.1. Observational site characteristics

Delhi is a place situated in the vast northern plains of India. Delhi ridge, one of the arms of the triangle wherein Delhi is located, is the north-western extension of the Aravali chain of hills. River Yamuna, another arm of this triangle, passes through the city in the western flank from north to south towards Agra. The soil is both rocky and agricultural. Delhi is the capital city and is thickly populated with industries scattered all over the city. Climate of Delhi is typical tropical, semi-arid type with severe summer and pronounced winter. Rainfall is light. SODAR was operated at CSIR-NPL located in central Delhi.

3.2. Different layers in SODAR echograms

The atmosphere of Earth is a layer of gases surrounding the planet Earth that is retained by Earth's gravity. The atmosphere protects life on Earth by absorbing ultraviolet solar radiation, warming the surface through heat retention (greenhouse effect) and reducing temperature extremes between day and night (the diurnal temperature variations). More than 6000 SODAR echograms have been recorded at the observation site, i.e., Delhi for different seasons were analyzed and classified into different categories. Figure 3.1 shows the multilayer, rising layer, Thermal plume, Waves and perturbations and Stratified layer echograms.

In figure 3.1(a), exhibits the multilayer types of echograms,which were obsered during night time. The mostly occurrence of Elevated layer or multilayer in the month of may and less occurrence in

the post-monsoon months i.e., october and november. According to seasonal, mostly occurrence in pre-monsoon and less in post-monsoon. The height of multilayer goes upto 600 meters, but normally height is upto 250 to 400 meters.The thickness of multilayer is from 10 to 150 meters, but generallyit is upto 60 meters (obersvation from 1stdecember to 30th november).

The inversion layer (figure 3.1(b)) structure which is a characteristic feature of the night time stable conditions dissipates in the morning after sunrise as a result of solar heating of the ground and the temperature profile changes its shape. The time taken for an inversion layer to dissipate after sunrise varies from day to day and season to season depending upon the presence of cloud cover, the strength of the inversion layer formed during the night, influx of solar heat and the presence of elevated layer or fog layer.

The nocturnal inversion while dissipated shows its presence in the form of a rising layer, reaches to a certain maximum height and then disappears. This type of structure is not seen daily in the morning time. A direct transition of the inversion layer to the plume structure takes place sometime. On the days under the rainy spell and cloud cover, the inversion layer does not show a rise layer. Therefore, in the season of monsoon, rising layer is formed less.

Studies of duration of the rising layer to various months, to see the different weather condition, rising inversion takes longer time during the winter months compared to the summer months. Also says that, rise rate is faster in the summer and slow in the winter season due to temperature profile change in the season of summer and winter.

Thermal plume structure (figure 3.1(c)) is a daytime structure and is associated with solar heating of the ground with the day break. The plume starts forming early in the morning when the surface inversion dissipates. With more and more heat, thermal plumes height also increases. According to months or season, the height of thermal plumes is more in the month of May or in the summer season. The duration of thermal plumes is maximum in the summer (pre-monsoon) and less in the winter.

Waves and perturbations (figure 3.1(d)) are another class of thermal plume structures which have been observed and classified directly on the SODAR echograms. A study of this type of structure in terms of observation, mostly observed in the months of April, May and June, according to season

mostly in pre-monsoon and less in the post-monsoon. This type of structure is important in the study of wave motion.

No degree of turbulence is detected unless air layers are present with gradients in the potential acoustic refractive index. In statically stable air, the vertical gradient of potential temperature guarantees the generation of temperature irregularities in the presence of turbulence. Shears in the mean flow built up in association with layers of enhanced static stability and increased temperature variability will be a consequence of dynamic instability and turbulence and will result in stably stratified shear layers out living small to medium scale atmospheric configurations. Horizontally stratified layers (figure 3.1(e)) in the lower atmosphere under statically stable conditions on land as outlined above have been observed by CSIR-NPL developed SODAR.

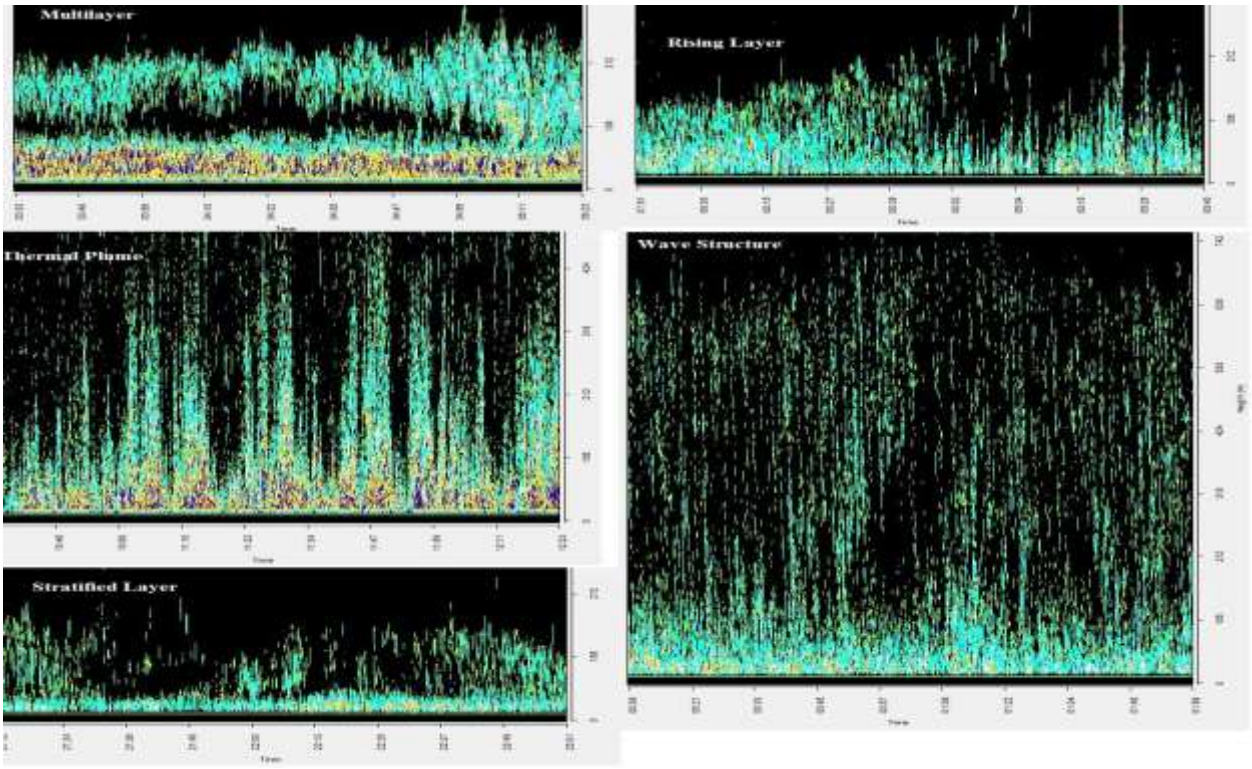

Figure 3.1. Different layers in SODAR echograms. (a) Multilayer, (b) Rising layer (c) Thermal plume (d) Wave structure (e) Stratified layer

3.3. Inference from Echogram

In general, seasonal changes have not been found to influence the characteristics of thermal echoes, however certain situation like rain, storm, cloud cover etc. suppress plume formation. High wind speed reduces vertical mixing by convective activity and the height of thermal plumes. In case of

an elevated layer at a height when thermal plumes exist the mixing height is limited to the height of that layer.

Shear echoes forms after subsiding thermal plumes. It remains throughout the night and in the morning when earth gets heated up by the sun the shallow layer formed gets lifted and thermal plume starts forming. SODAR visualizes the changes in the pattern and height of the night time stable layer. In the case of shallow layers weather conditions have clear effect. Layer with plain top formed in the low wind conditions or with no wind. Thickness of this layer increases if this condition persists. Surface wind brings mixing in the stable layer, the spikes on the structure shows gustiness of the wind. Sometimes multilayered structure forms above the surface based layer. The layers have features of sinusoidal motion in clear weather conditions and sharp vortex in turbulent weather conditions. Dot echo structure above the surface based layer indicates water vapor. It is observed in moist conditions soon after rain or evenings in rainy season. Fog forms a shallow surface layer in winter months. Calm wind, clear skies and fairly high relative humidity favors occurrence of fog.

3.4. Typical SODAR Observations

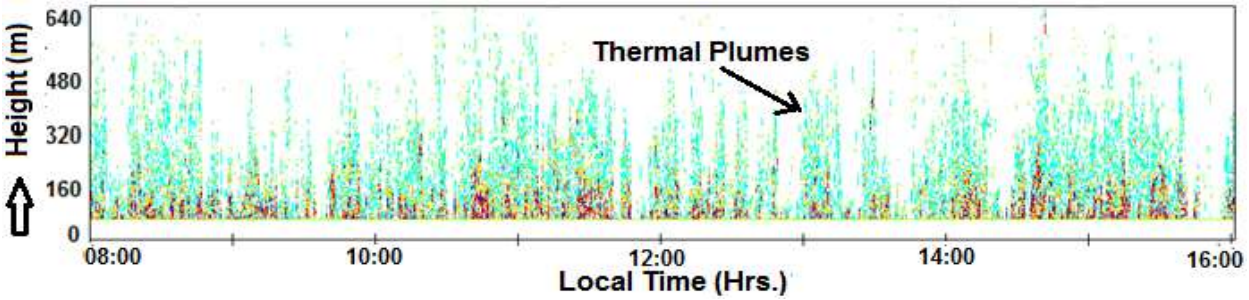

Figure 3.2. Clear Sunny day in summer

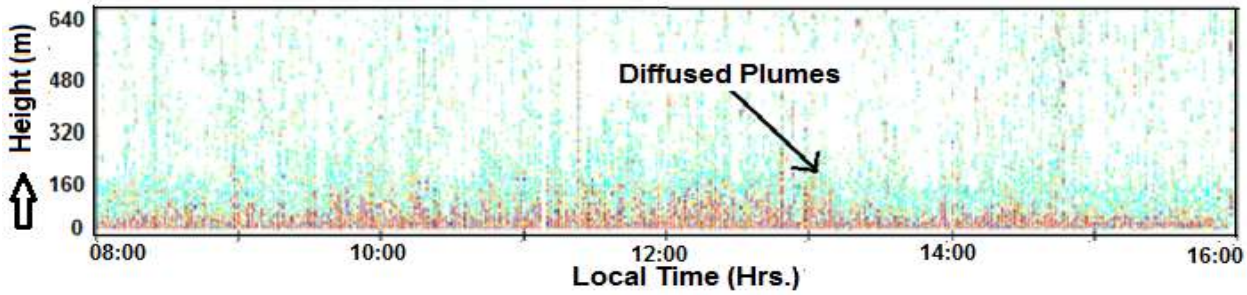

Figure 3.3. Strong winds on clear sunny day

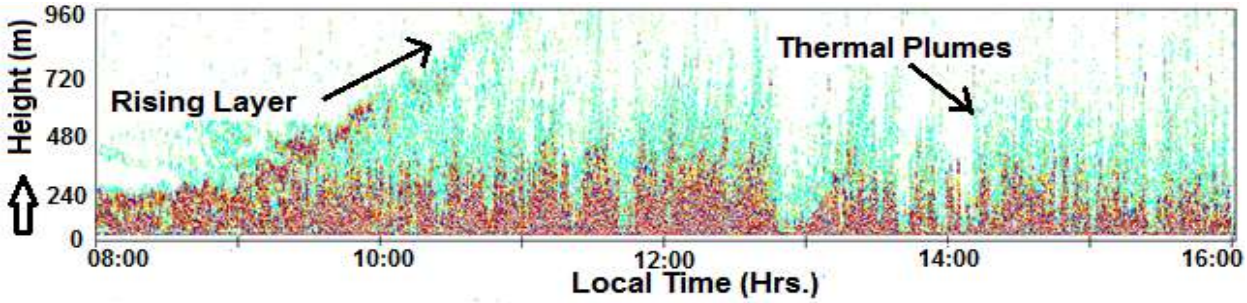

Figure 3.4. Clear Sunny day in winters

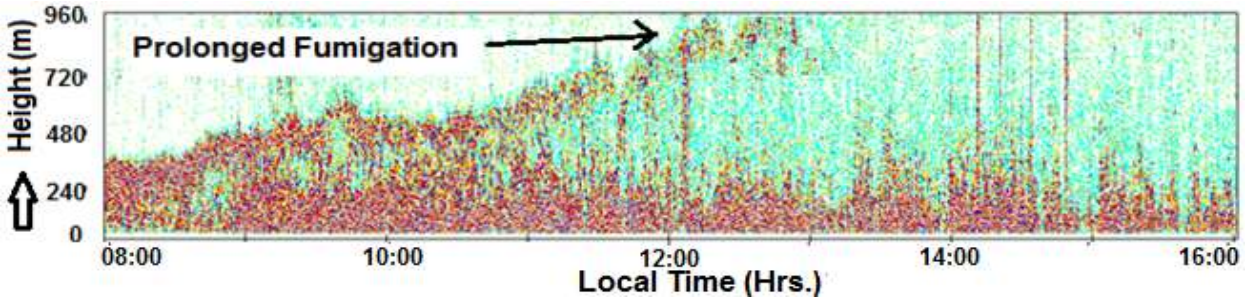

Figure 3.5. Fumigation

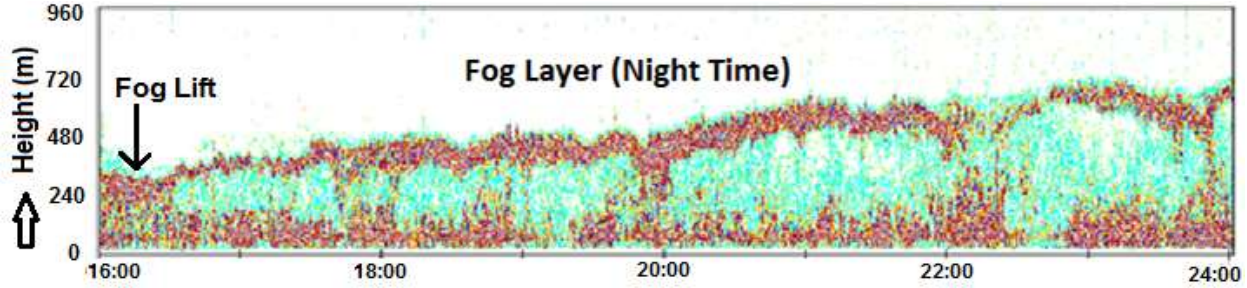

Figure 3.6. Fog formation at night time

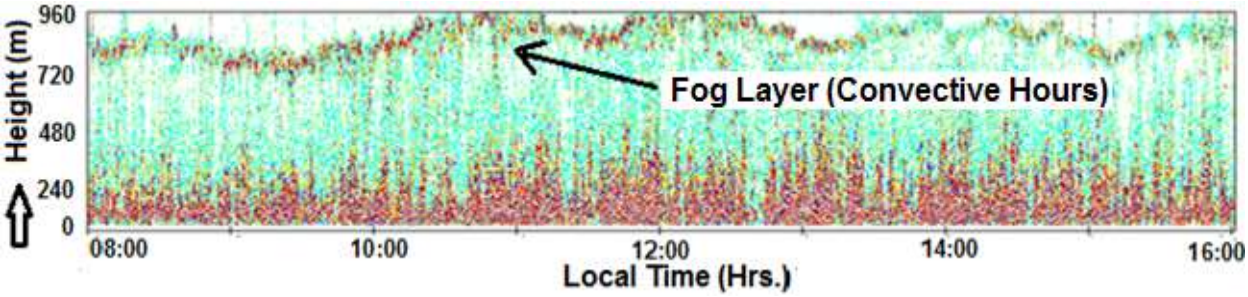

Figure 3.7. Fog Layer at day time

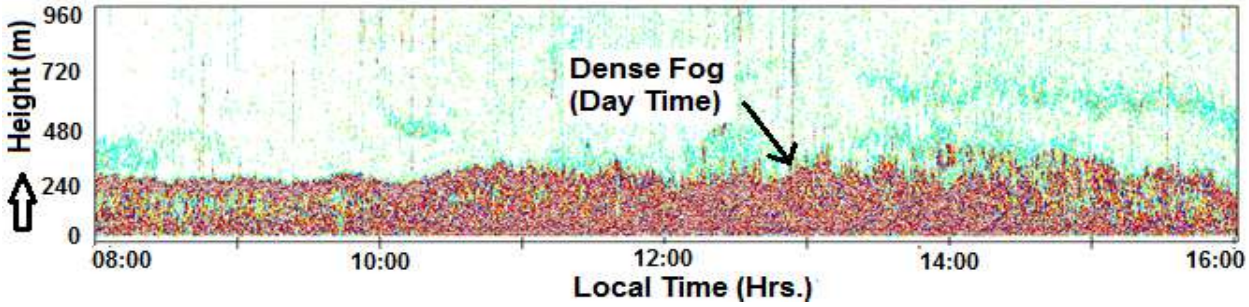

Figure 3.8. Fog dense at day time

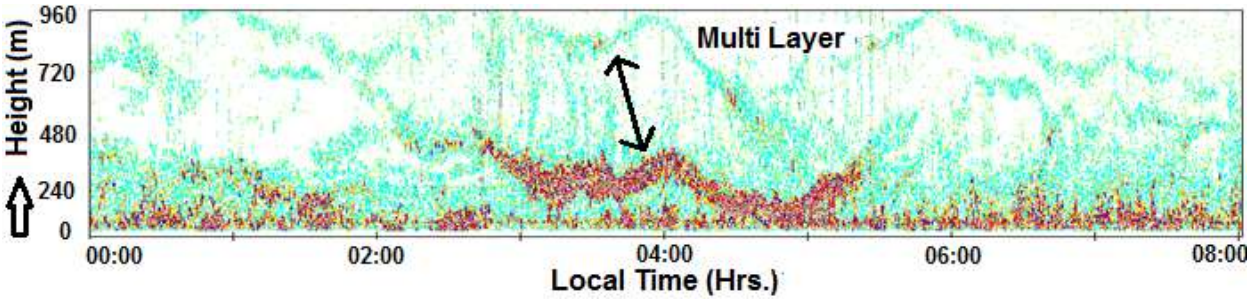

Figure 3.9. Multi-layered structure in stable atmosphere - winter morning

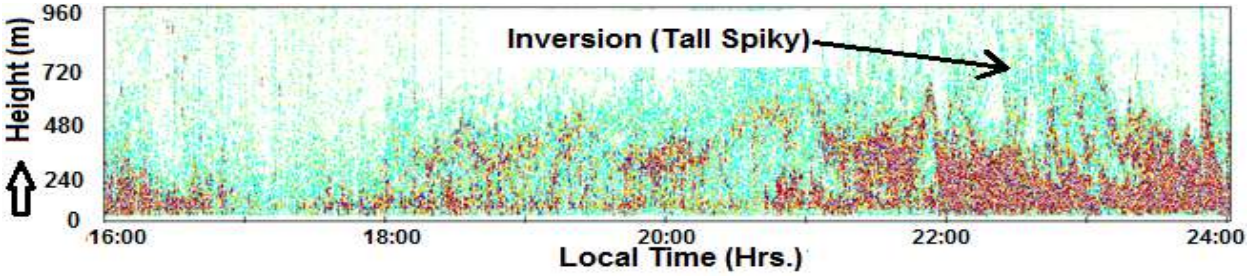

Figure 3.10. Inversion with strong wind

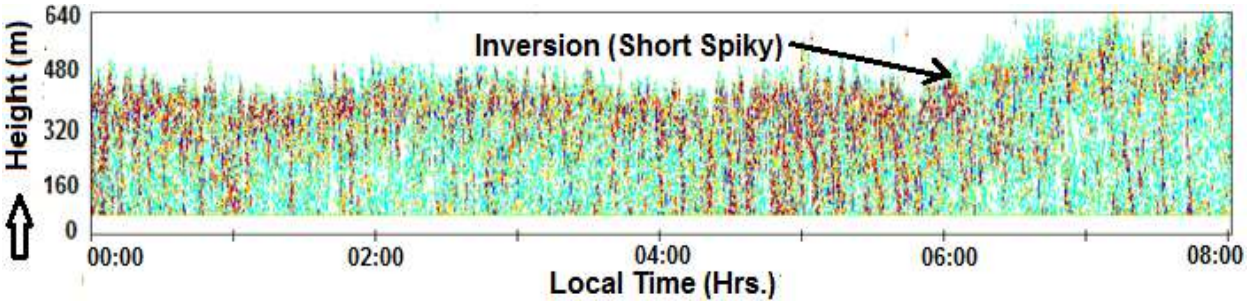

Figure 3.11. Inversion with wind

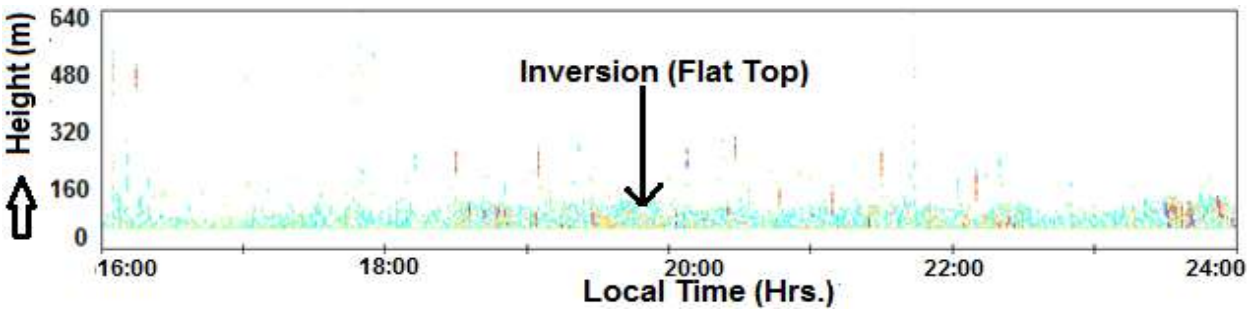

Figure 3.12. Inversion with no wind

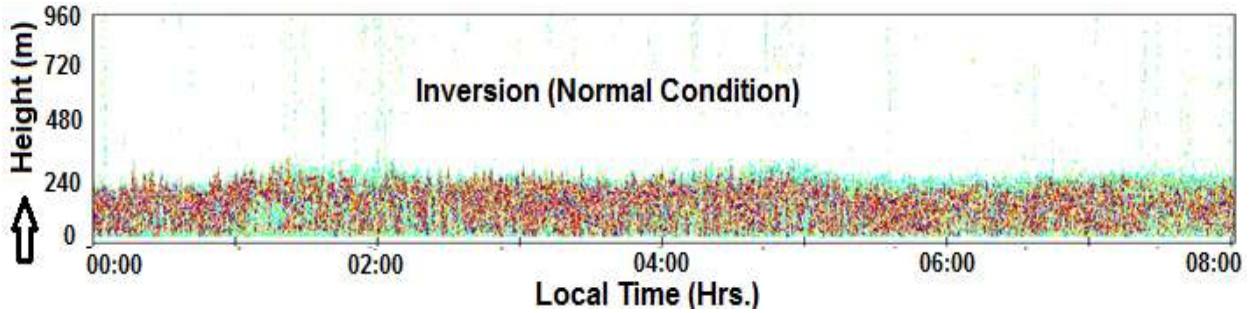

Figure 3.13. Normal condition at night time

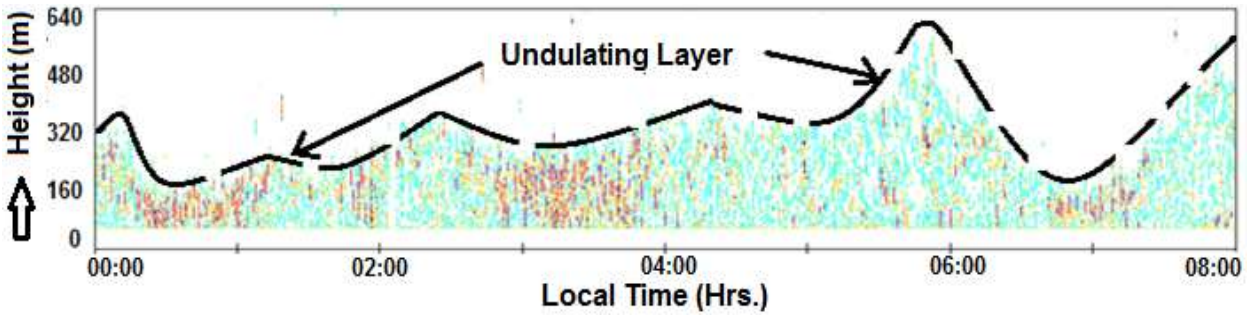

Figure 3.14. Layer when there is fluctuation in wind speed

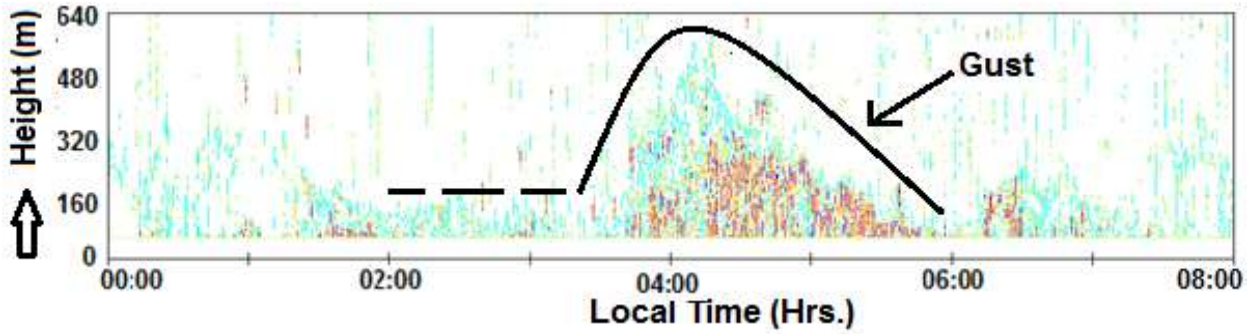

Figure 3.15. Surface based layer with a gust

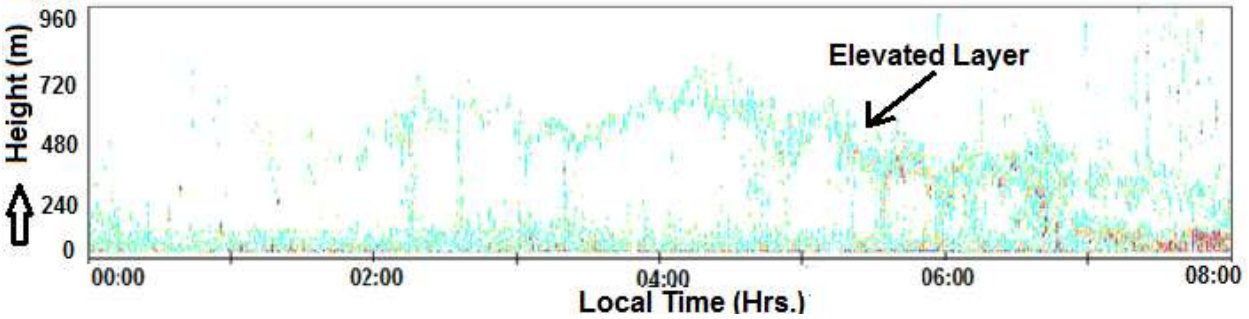

Figure 3.16. When a stable layer exists at a height

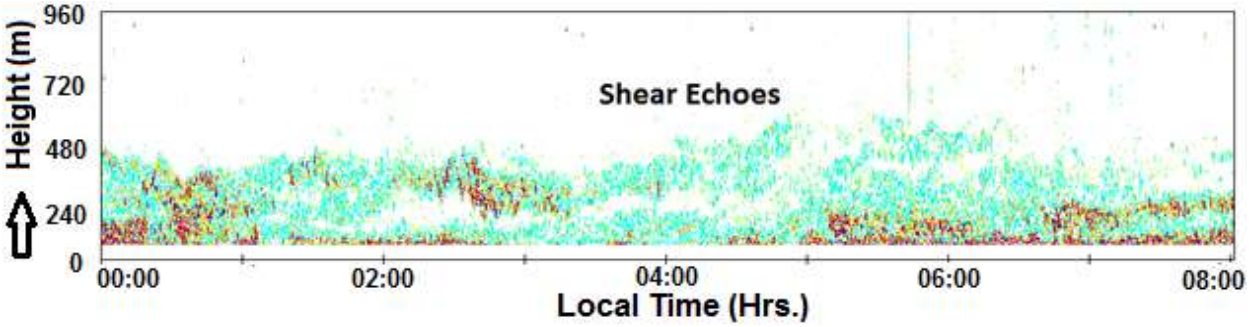

Figure 3.17. Wind influenced stable layer

3.5. Annual, seasonal and temporal variation of Mixing Height

Qualitative indicators of the stable and unstable ABL conditions are respectively the presence of inversions and thermal plumes. The atmospheric mixed layer is a zone having nearly constant potential temperature and specific relative humidity with height. The depth of the atmospheric mixed layer is known as the mixing height. Mixing height is also known as the height of the layer getting mixed up by solar height (convection) or mechanical turbulence within one hour. From a mixing height, determines the volume available for dispersion of pollutants and characterizes the structure of the lower atmosphere. Higher the value of mixing height, the greater is dispersion rate and vice versa.

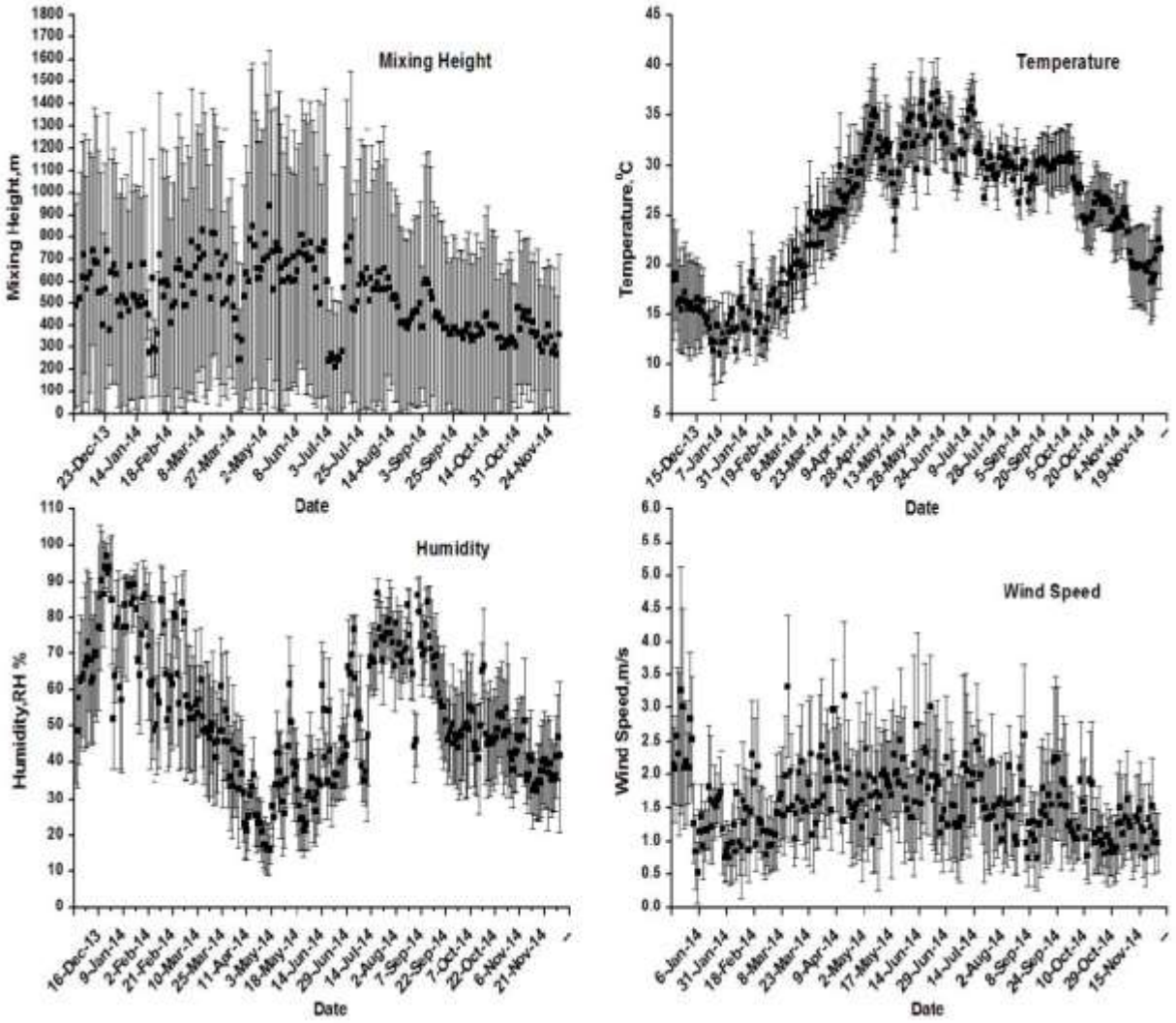

Figure 3.18. Daily average variation of mixing height and meteorological parameters from Dec. 2013 to Nov 2014

Based on the observation of SODAR echograms, the mixing height of ABL is changing continuously. Figure 3.18. represents the annual variation of mixing height (draw using Origin 6) due to atmospheric condition (like temperature, relative humidity, wind speed, etc.). Also figure 3.18. represents the annual variation of temperature, relative humidity and windspeed.The vertical bars denote the ± σ standard deviation from the daily mean. It repesents, mixing height is a positive correlation with temperature and wind speed, whereas with relative humidity its shows negative correlation. The average values of mixing height, temperature, wind speed and relative relative humidity during the whole day were found to be 530±155m, $25^0 \pm 7^0$C, 1.53±0.70 ms^{-1}, 53±18 % RH respectively.

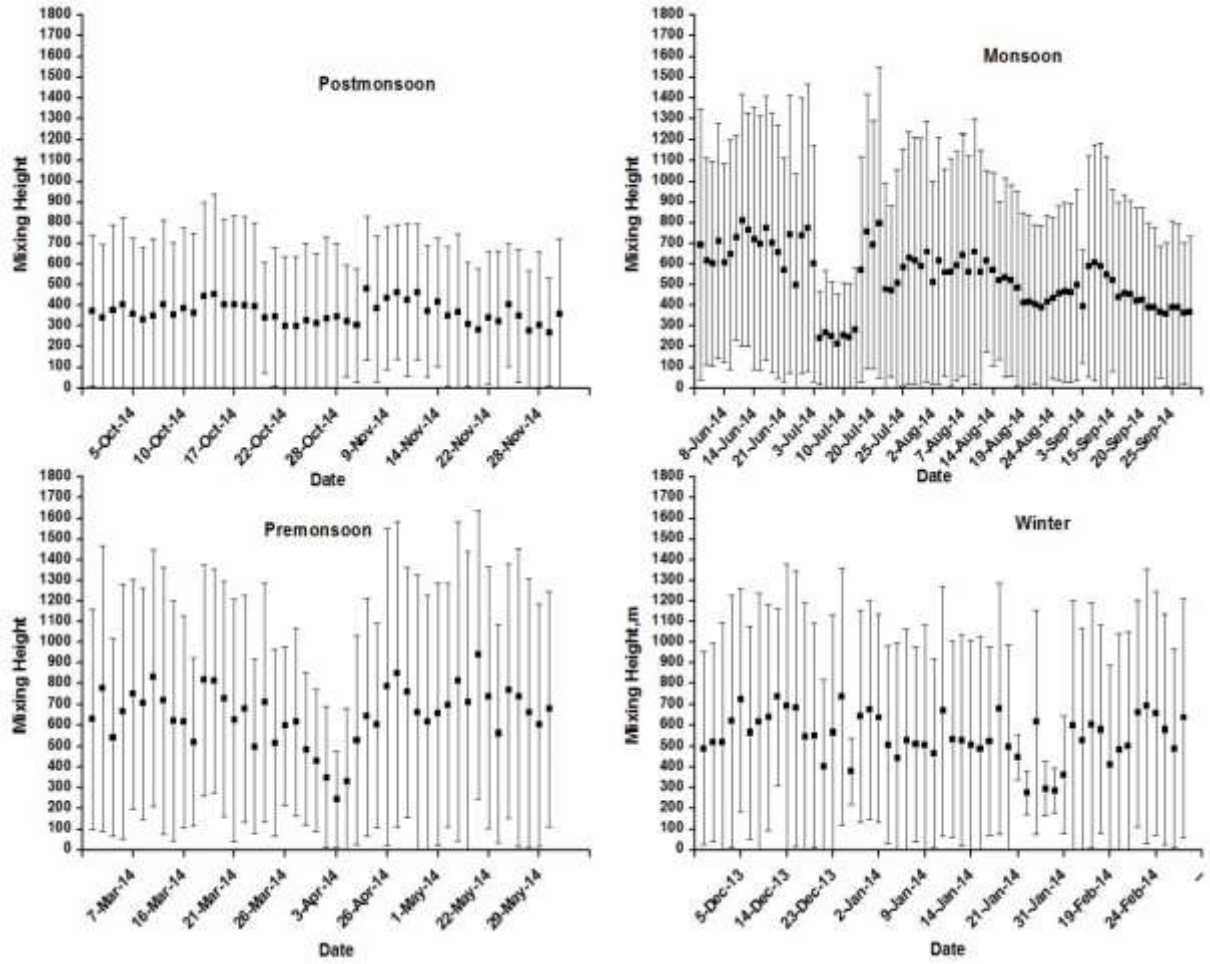

Figure 3.19. Daily average seasonal variation of mixing height from Dec. 2013 to Nov 2014 during different seasons. (a) Postmonsoon,(b) Monsoon, (c) Premonsoon, (d) Winter

Daily average SODAR data for about one year for all months (from December 2013 to Novmber 2014) are analyzed to derive the mixing height. The total data set has been classified into four seasons namely winter (December-January-February), Pre-monsoon (March-April-May), Monsoon (June-July-August-September) and Post-monsoon (October-November) on the basis of meteorology over northern India. The seasonal variation of mixing height during the whole year of observationhas been shown in figure 3.19 (draw using Origin 6). According to figure 3.19, In Pre-monsoon, mixing Height is maximum approx 1700 meters, whereas in Post-monsoon, mixing height is approx 950 meters. The daily average values of mixing height during the four seasons,winter, pre-monsoon, monsoon and post-monsoon were found to be 555±115m, 650±145m, 535±145m, 365±50m respectively. The present observation shows that though the maximum mixing height was in pre-monsoon and minimum in post-monsoon at Delhi.

3.6. Relation between Mixing Height and Meteorological parameters during different Seasons

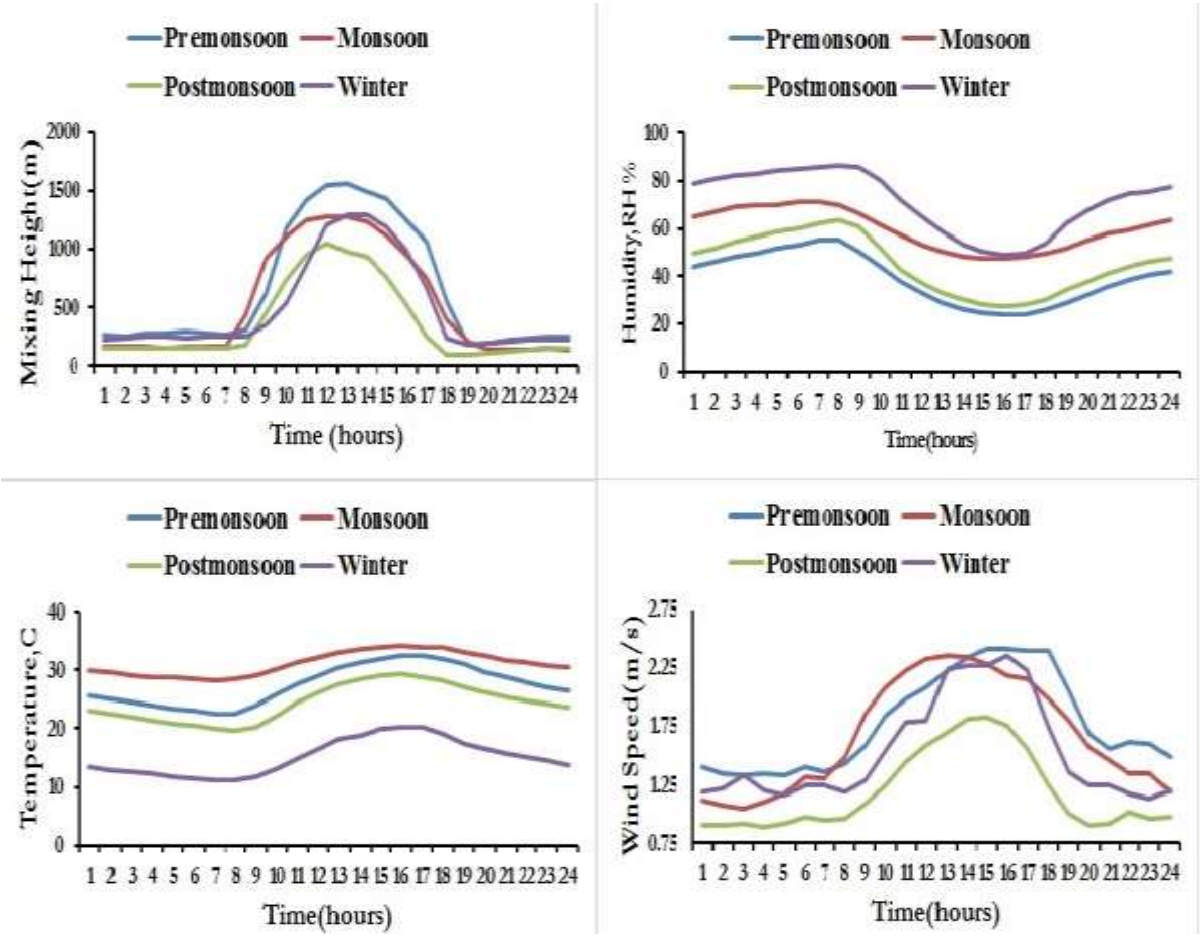

Figure 3.20. Temporal variation of mixing height and meteorological parameters during different seasons. (a) Mixing height, (b) Humidity, (c) Temperature, (d) Wind speed

Figure 3.20. shows, temporal variation of mixing height, temperature, windspeed and relative humidity during the different seasons (draw using Microsoft excel 2013). Mixing height has positive correlation with temperature and wind speed, whereas negative correlation with relative humidity. Figure 3.20. represents that, when temperature and windspeed were increased, then mixing height was also increased, whereas when relative humidity was decreased then mixing height was also increased. The temporal average values of mixing height during the four seasons,winter, pre-monsoon, monsoon and post-monsoon were found to be 555±115m, 650±145m, 535±145m, 365±50m respectively. The corresponding value of temperature ,windspeed and relativehumidity are given in table 3.1.

Table 3.1. Temporal variation of mixing height and meteorological parameters during different seasons

	Winter	**Premonsoon**	**Monsoon**	**Postmonsoon**
Mixing Height,(m)	555±115	650±145	535±145	365±50
Temperature,(^{0}C)	15±3	27.5±3.5	31±2	24.5±3
Wind speed,(m/s)	1.52±0.44	1.77±0.41	1.67±0.48	1.18±0.34
Humidity, (% RH)	71±13	39±10.5	60±8.5	45±12

Temperature and wind speed are influencing positively to the mixing heights during all the seasons. The convective boundary layer height advances and decreases during the day time depending on the increase and decrease of surface temperature due to solar heating of the ground. The variation in surface temperature controls the existence of atmospheric convection; therefore it strongly affects the mixing height. The negative correlation has been observed between mixing height and relative humidity (RH), indicates that as the relative humidity increases mixing height decreases.

Generally, it is high in between 11:00 A.M. to 14:00 P.M. in all seasons. After that, mixing height is decreasing due to decrease in solar heat. The highest mixing height during convection period was approx 1550 m, 1495 m, 1280 m, 1050 m during pre-monsoon, winter, monsoon and post-monsoon seasons respectively.

CHAPTER 4

STUDY OF STABILITY CLASS AND ITS VARIABILITY IN DIFFERENT SEASON

4.1. Introduction

It is a well-known fact that transportation, dispersion and diffusion characteristics in the atmosphere depend on the mixing depth of the atmospheric boundary, its stability conditions, mesoscale flow pattern and wind characteristics. Therefore, knowledge of these air pollution concerned meteorological parameters becomes essential to determine the air quality at a place. Atmospheric stability is a measure of the prevailing turbulence strength which ranges over a broad spectrum. It ranges from vigorous turbulence (extremely unstable ABL) to nearly no turbulence (extremely stable ABL) conditions.

ABL height is change in temperature, relative humidity, wind speed, wind direction and solar heating, etc. The degree of stability of the atmosphere must be known to estimate the ability of the atmosphere to disperse air pollutants. To find the out the atmospheric stability, different methods are available, for example Richardson number, Pasquill-Gifford stability classification, Pasquill-Turner stability classification, mixing height, stability classification etc. are used. These different methods have different quality to define the stability with respect to convection and mechanical turbulence. During the 24 hours, in a daytime, the atmospheric condition is continuously changing, due to this stability class of the atmosphere is also changed, whereas in afternoon stability class is in unstable condition, generally during sunset it is almost neutral and in night time it is stable. Consequently, continuous monitoring of ABL is essential and it is possible only from SODAR remote sensing technique.

4.2. Unstable Atmospheric Boundary Layer

The turbulence in the lower atmosphere is responsible for dispersion of the emissions and it also serves as tracers for generating SODAR signals. Therefore, a measure of the vertical height of the turbulent region of ABL gives a direct measure of the mixing depth for the emissions released near the ground.

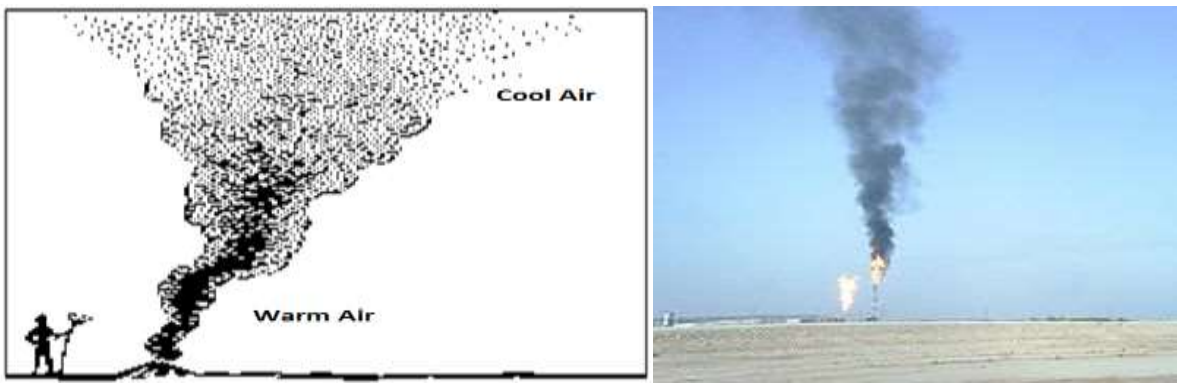

Figure 4.1. Unstable Condition at day time

This turbulent region is mapped as the thermal plumes (on SODAR echograms) during day time (Figure 4.2).

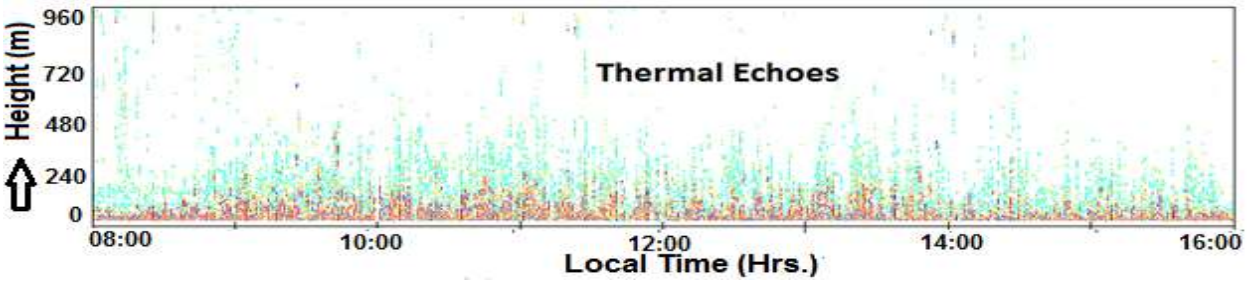

Figure 4.2. Thermal Echoes

However, it may be pointed out that a measurement of the height of the thermal plumes during day time by SODAR gives an under-estimate value as it is a function of the SODAR sensitivity in relation to the prevailing ambient noise which is high enough during day time as compared to night time. A true measure of the unstable ABL mixing depth can only be made in case thermal plumes are capped by a shear echo / inversion layer (Figure 4.3).

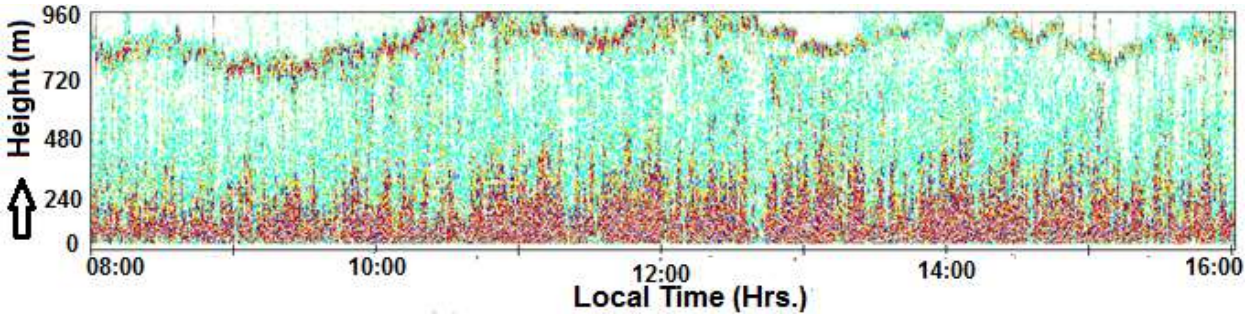

Figure 4.3 Thermal plumes capped by inversion layer

The observed height of the thermal plumes is the most active mixing height during day time. Based on the correlation studies of the SODAR observed height of the thermal plumes and the actual mixing height computed through Holzworth model (using the simultaneous SODAR and radiosonde observations made at IMD, Aya Nagar, Delhi by S.P. Singal) an empirical relationship has been worked out to determine the actual height of convective boundary layer knowing the SODAR observed height of the thermal plumes. The said relationship, given below, is used in the present work.

$$\text{Mixing Height, MH} = (4.24\ P_h + 95) \text{ meters}$$

where P_h is the plume height (in meters) as observed on SODAR echograms. It may be mentioned that the SODAR echoes, at any site, are the manifestations of the resultant of turbulent conditions caused by interaction of topographical features and several prevailing meteorological factors via: wind, vertical transfer of heat, mass, momentum, moisture etc. As such the effect of various site specific parameters gets embedded in the resultant upward heat flux which in turn is translated into observed height of SODAR structure.

4.3. Stable Atmospheric Boundary Layer

Shear echoes represent regions of stable conditions, with their height measuring mixing height in the stable layer. The precise height of shear echoes is determined from the intensity profile of SODAR returns of each sweep, using an off line program.

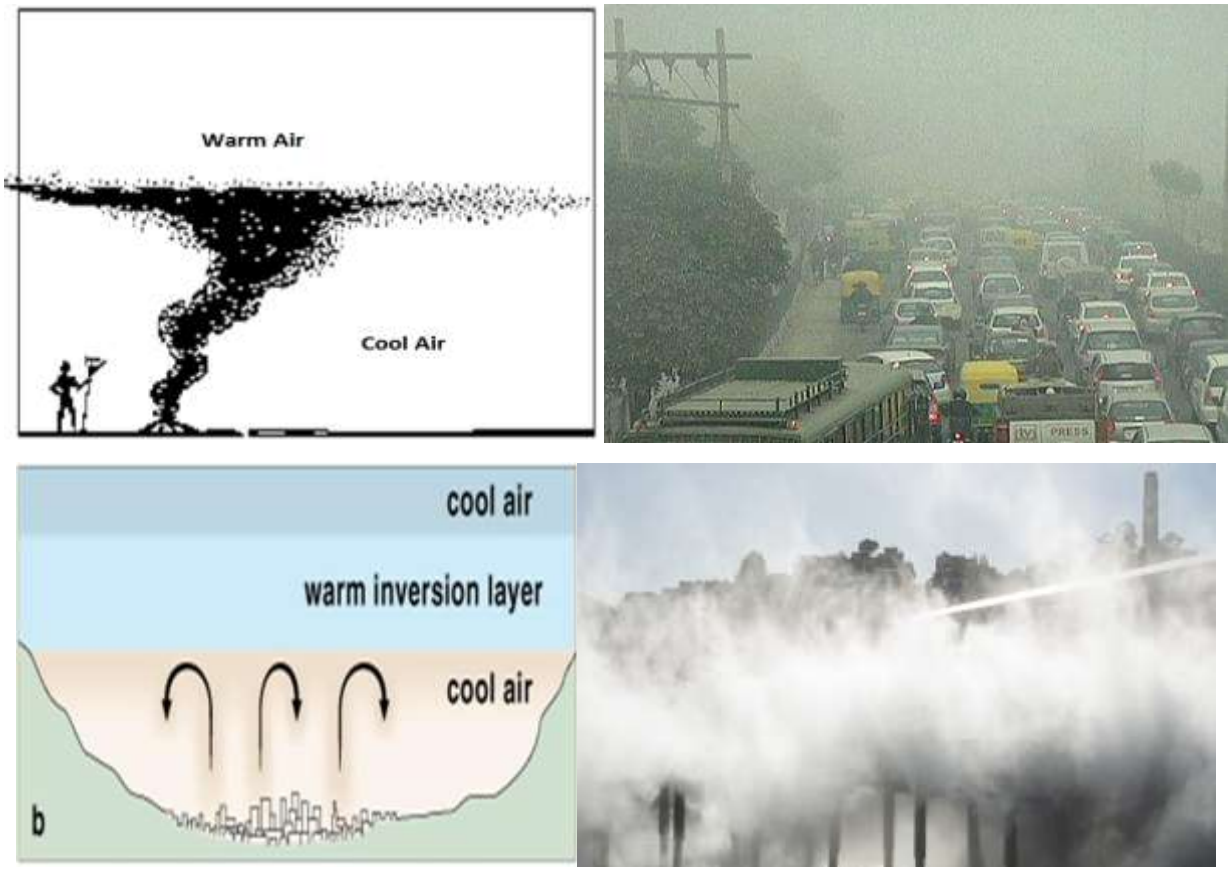

Figure 4.4. Stable Conditions

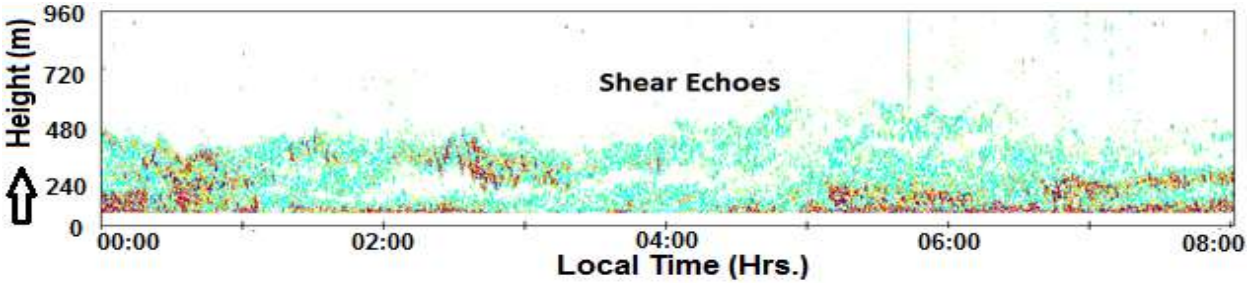

Figure 4.5. Shear echoes

Under stable ABL conditions, the height of ground based shear echoes or the flat / spiky top layer gives a fairly good estimate of the mixing height. In the present case, the SODAR probes the ABL at sweep rate of 6 sec. The received signal (or the digital data) is processed, online, to produce echograms showing pictorial view of the dynamics of the meteorological phenomenon prevailing in the ABL.

An offline computer program, based on SODAR pattern recognition and the criterion lay down for mixing height determination under different meteorological conditions, is used to derive mixing

height values using the digital data file. The program computes one value of the mixing height from each sweep of received signals. Confining ourselves to the requirement of hourly mixing height studies, 600 values of mixing height are obtained in each hour of the day. These 600 values are averaged to obtain one hourly mean value of mixing height.

4.4. Atmospheric Stability Classes

SODAR echoes represent the turbulent regions of the atmosphere, and extend of the SODAR echoes have been used to broadly characterize the general state of the atmospheric stability via: stable, unstable and neutral however, practical application for air quality studies requires quantification of turbulence through estimation of Pasquill stability class rather than knowledge of stable or unstable condition only.

Several attempts have been made to correlate SODAR structural details and the six Pasquill stability classes (A to F) which are derived by the standard methods using simultaneous measurements of meteorological parameters of wind speed, wind direction, temperature gradient, bulk Richardson number, solar radiation, cloud cover standard deviation of wind direction etc. It has been shown that SODAR derived stability classes are in fairly good agreement with those derived by conventional methods for practical purposes. In pursuit of the same, based on correlation studies of the site specific observed echoes and the SODAR derived variance of vertical wind velocity at CSIR-NPL, a scheme has been worked out to derive stability class using SODAR structural details.

In normal clear days, the stable categories (E& F) of the ABL exist mostly during night time when SODAR maps a ground based layer with flat / spiky top. The unstable category (A, B, C) exists during day time when SODAR records thermal plumes showing height variation in accordance with solar heating of the ground and related lapse rate profile. However, the neutral stability can exist both during day and night time depending upon the prevailing meteorological conditions. It is seen as occurring more specifically, around sunset hours in the evening when the transition from unstable to stable ABL takes place. This transitional period or the neutral stability is marked as a blank record or no echo structure on SODAR record. Besides, the strong surface winds which make the facsimile record totally dark all through its height also depict the duration of near neutral conditions. Thus, the broad stability (stable, unstable or neutral) can be inferred from appearance of ground based stable layer, thermal plumes and no echo structure on SODAR records. However,

sub-classification of stability is determined from finer structural details in terms of height and superimposed additional structures / complexities *etc*. It may be mentioned that the SODAR based classification scheme for stability class A, B and C (pertaining to the unstable ABL) is plume height dependent. Heights to which plume echoes are visible on a sounder facsimile record depend on the background noise level, the sensitivity and transmit acoustic power of the sounder. Moreover, the true height to which thermal plumes would rise depends on the prevailing temperature gradient and the intensity of turbulent temperature fluctuations within rising thermal plumes. The details of the classification scheme given in Table 4.1 are based on use of SODAR developed at CSIR-NPL. The scheme has been used for stability studies in the present work. Broad features of the classification scheme can be summarized as follows:

Class A, representing strongly unstable conditions, is marked on the SODAR echograms by well-defined families of tall thermal plumes.

Class B, representing moderately unstable conditions, is marked on the SODAR echograms by thermal plumes of moderate height.

Class C, representing slightly unstable conditions, is marked on the SODAR echograms by very shallow plumes formed during the early morning and late afternoon hours, cloud cover, foggy weather conditions etc.

Class D, representing near neutral conditions, is marked on the SODAR echograms either by no structure or by dark bands due to strong wind induced noise.

Class E, representing slightly stable conditions, is marked on the echograms either by a ground based horizontal layer of higher depth or by the tall spiky layer structures during the night time.

Class F, representing moderately stable conditions, is depicted on SODAR echograms either by shallow and flat top ground based layer or by shallow stratified layer structure or presence of elevated and wavy layers in addition to ground inversion.

Table 4.1: SODAR based stability classification scheme

Local Time	SODAR structure	Stability Class
0500-1000	Stable layer (>150m) Stable layer (<150m) Rising layer Elevated layer/or multi-layers/or waves (200m) ≥ Convective plumes (≥125m) Convective plumes (<125m) No structure	E F C F B C D
1000-1800	Rising layer Convective plumes (≥200m) Convective plumes (125-200m) Convective plumes (≤125m) No structure Stable layer Stable layer with elevated layer /waves Elevated layer with plumes below Stable layer	C A B C D E F C
1800-2100	No structure Stable layer with flat top/short spikes Stable layer with tall spikes (≥300m) Stable layer with wavy top Elevated layer/waves	D E D F F
2100-0500	No structure Stable layer with flat top (<125m) Stable layer with flat top (≥125m) Stable layer with spikes (≥300m) Stable layer with wavy top Elevated layer	D F E D F F

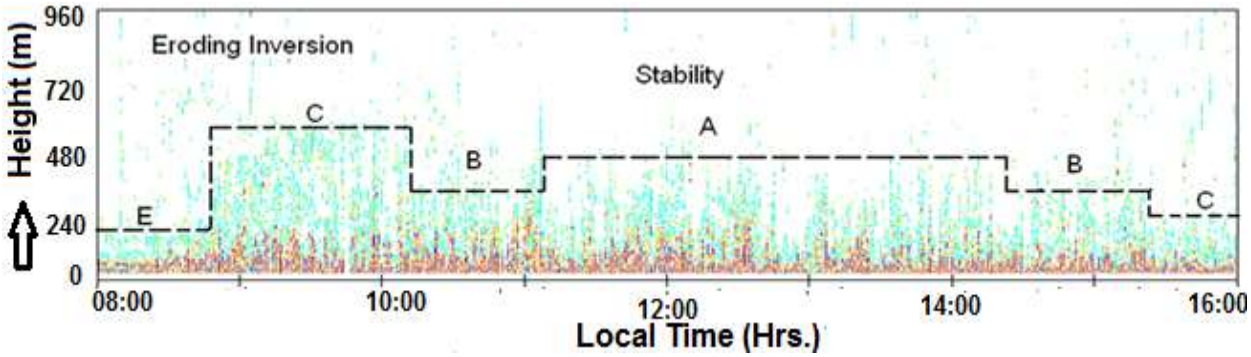

Figure 4.6. Normal variation of stability class under clear weather in summers

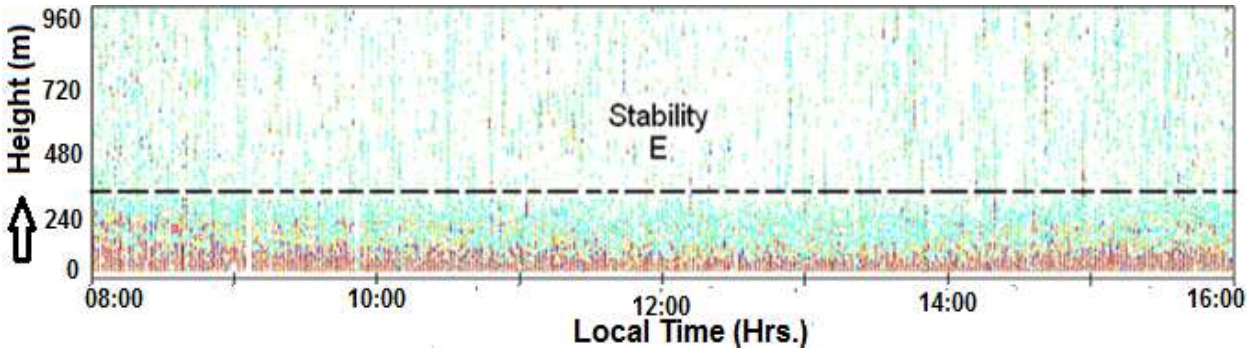

Figure 4.7 Deviations in the observed variation of stability class under disturbed weather conditions in summers

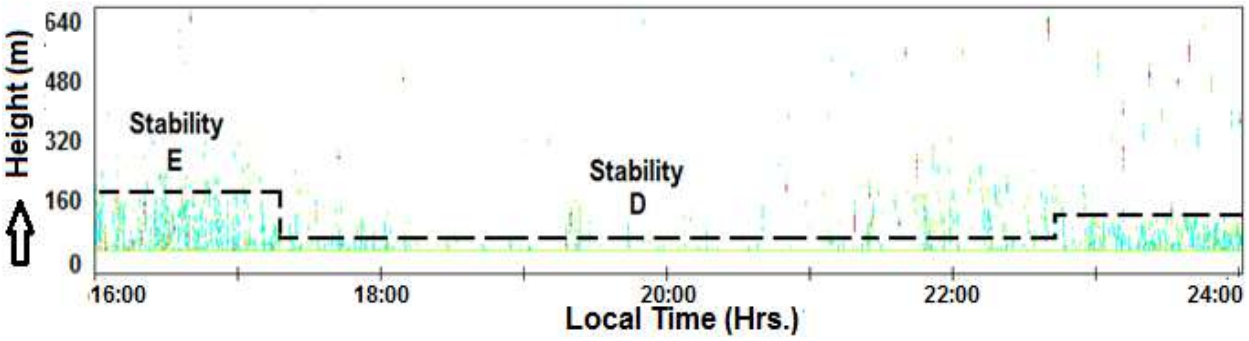

Figure 4.8. Observed variation of stability class under disturbed weather conditions in winters

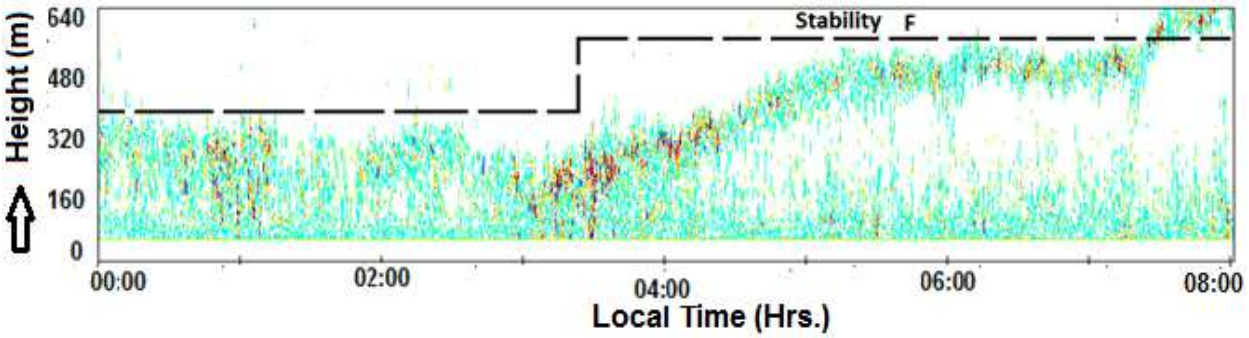

Figure 4.9. Observed variation of stability class under disturbed weather conditions in winters

At any given location or region the value of mixing height may be greatly affected by the presence of meteorological parameters and their variation during different seasons. At Delhi, which is a highly polluted metropolitan city, most of the air-pollutants are either locally produced by extensive urbanization, industrialization, and construction activities, increased vehicular pollution, biomass burning or transported from large arid and semi-arid regions in north-west part of India.

In this chapter, the mixing height and their stability class have been estimated and plotted from SODAR echograms at Delhi during December 2013- November 2014 and relationship between stability class and atmospheric parameters (temperature, wind speed, relative humidity *etc*) during

the same period are also studied. The behaviors of stability class during different weather conditions like, clear, cloudy and foggy have also been discussed.

4.5. Determination of Stability Class at New Delhi

Atmospheric stability is a measure of the prevailing turbulence strength which ranges over a broad spectrum. It ranges from vigorous turbulence (Highly unstable PBL) to nearly no turbulence (Highly stable PBL) conditions. There are many attempted to develop an approach based on SODAR echo patterns to classify Pasquill stability categories.

There are divided the ABL into six categories of stability from A to F which can be classified on the basis of data of surface wind speed, wind direction, day time insulation, night time sky conditions and temperature lapse rate, developed an approach based on SODAR echo patterns to classify Pasquill stability categories.

The stability classes can be determined based on mixing height and SODAR echograms. There are classified it into six classes based on the classification. In the present chapter an algorithm based on LabVIEW has been developed to plot the stability class from A to F directly from mixing height data, which is shown in table 4.1. and figure 4.10.

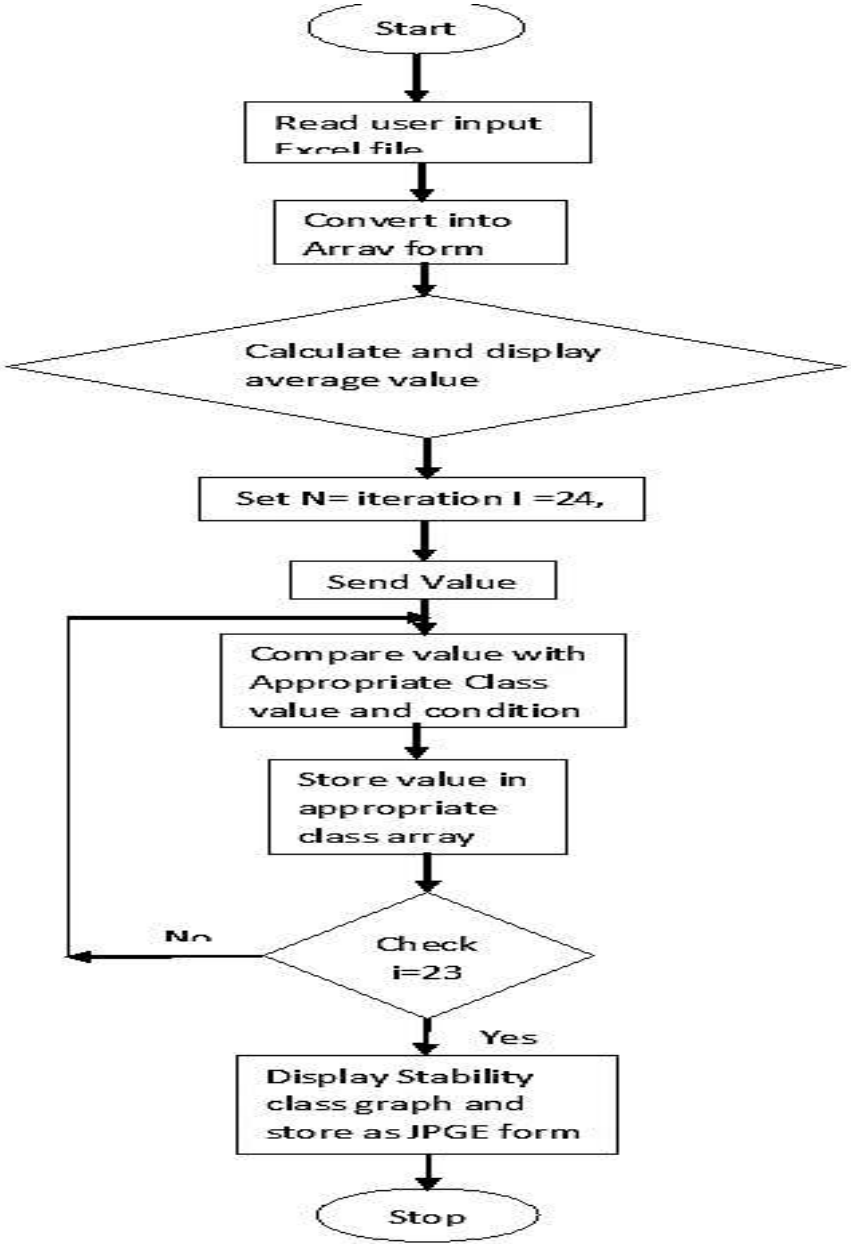

Figure 4.10. Flowchart representing the developed program for the stability class

4.6. Stability Class and its Seasonal and Temporal variability

Atmospheric stability is important for studies of air-pollution. Pasquill (1961) categorized it into six classes from class A to class F, however strong unstable, unstable, moderate unstable, neutral, stable, strong, stable are class A, class B, class C, class D, class E, class F correspondingly.

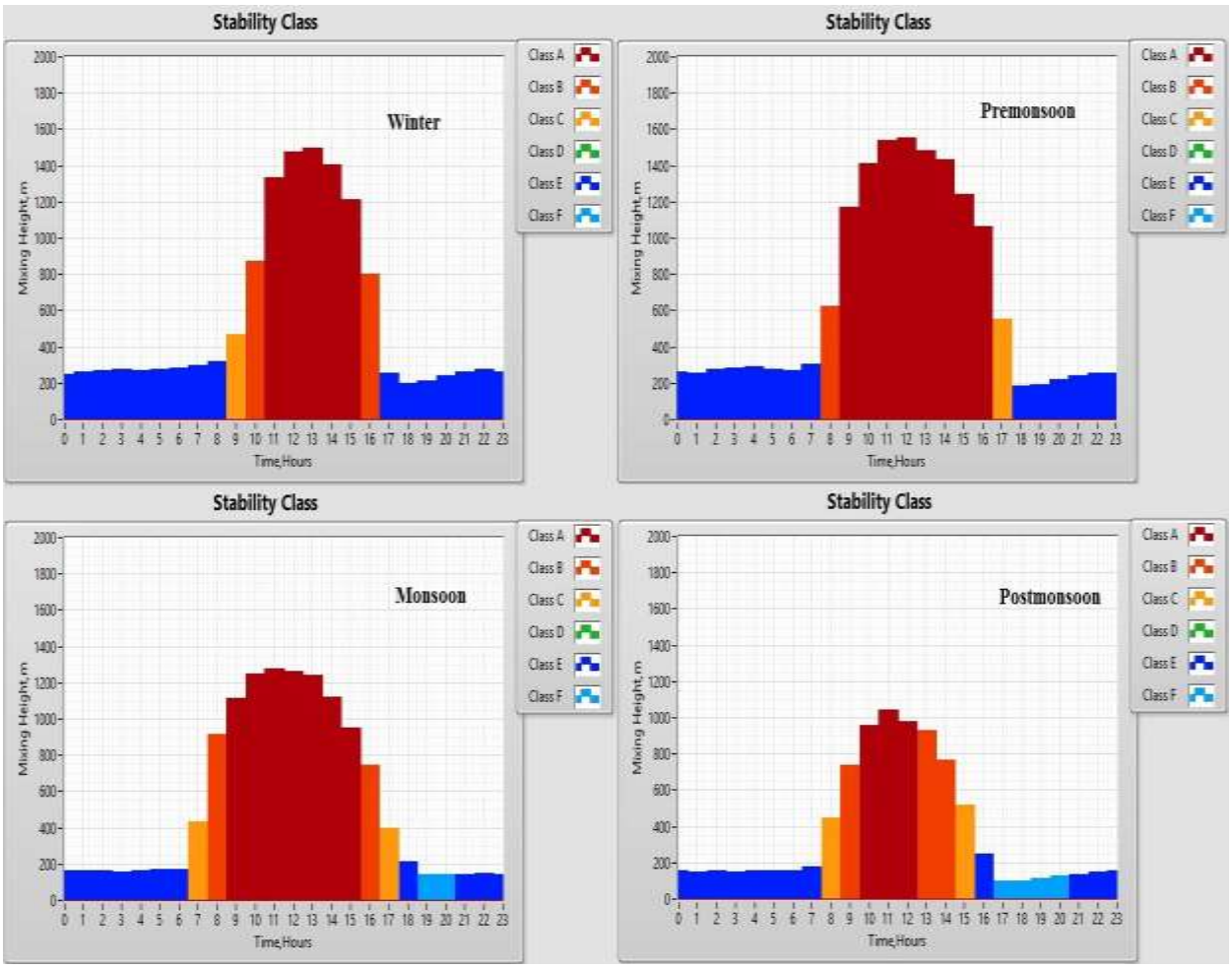

Figure 4.11. Stability class and its seasonal and temporal variability. (a) Winter, (b) Premonsoon, (c) Monsoon, (d) Postmonsoon

Using SODAR echograms and the information given in table 4.1., mixing height of Delhi city is classified as follows, which is shown in figure 4.11. Figure 4.11., shows temporal variation of stability class in different seasons. From table 4.2., it is observed that, Class A and Class E was dominated in convection and nocturnal periods in all seasons, whereas class F is absent in winter and pre-monsoon.

Table 4.2. Stability class for different Season of the periods at CSIR-NPL, New Delhi

Winter		Pre-monsoon		Monsoon		Post-monsoon	
Time	**Class**	**Time**	**Class**	**Time**	**Class**	**Time**	**Class**
00:00-09:00	E	00:00-08:00	E	00:00-07:00	E	00:00-08:00	E
09:00-10:00	C	08:00-09:00	B	07:00-08:00	C	08:00-09:00	C
10:00-11:00	B	09:00-17:00	A	08:00-09:00	B	09:00-10:00	B
11:00-16:00	A	17:00-18:00	C	09:00-16:00	A	10:00-13:00	A
16:00-17:00	B	18:00-00:00	E	16:00-17:00	B	13:00-15:00	B
17:00-00:00	E			17:00-18:00	C	15:00-16:00	C
				18:00-19:00	E	16:00-17:00	E
				19:00-21:00	F	17:00-21:00	F
				21:00-00:00	E	21:00-00:00	E

4.7. Stability Class in Different Weather conditions

Figure 4.12. represents, stability class in different weather conditions (i.e., clear day, cloudy day and foggy day). Figure 4.12(a) represents stability class of clear day, in this figure all stability classes are present. During the whole day the class A is dominated and in the midnight class D is dominated (due to tall spiky stable layer). Figure 4.12(b) represents stability class of cloudy days, in this figure class D is absent, where in mid-day the class B is dominated due to cloud and in night time class E is dominated. Similarly, figure 4.12(c) represents stability class of foggy days. During foggy days in the morning time, class E and class C occurred for a longtime after sunrise.

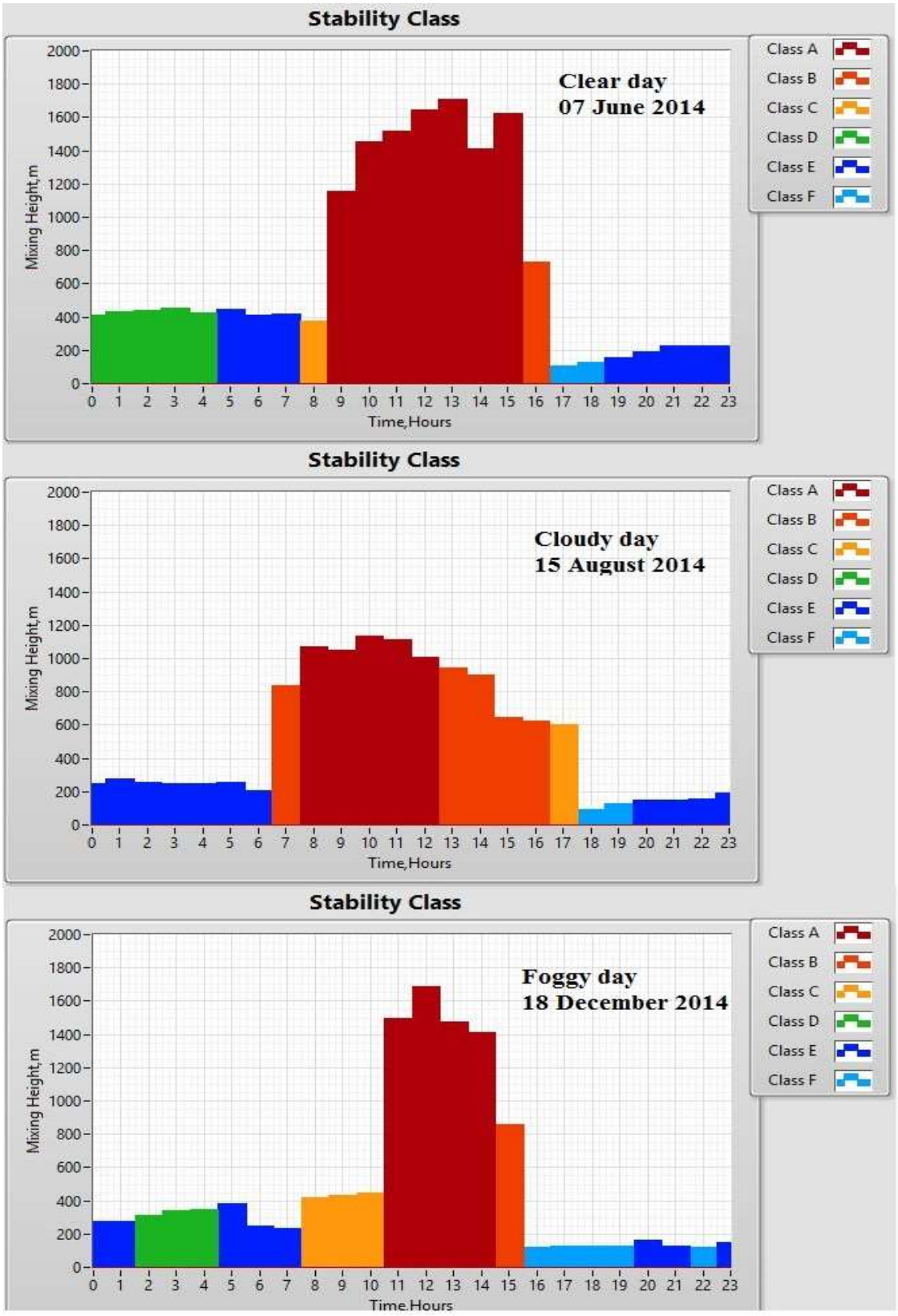

Figure 4.12. Different day stability class. (a) Clear day (b) Cloudy day (c) Foggy day

Table 4.3 Clear Day (7 June 2014)

Hours	SODAR Structure	Class
00:00-05:00	Tall spiky stable layer	D
05:00-08:00	Stable layer	E
08:00-09:00	Rising layer	C
09:00-16:00	200m< thermal plumes	A
16:00-17:00	200m> thermal plume	B
17:00-19:00	Unstable to stable state	F
19:00-23:59	condition Stable layer	E

Table 4.4 Cloudy Day (15 August 2014)

Hours	SODAR Structure	Class
00:00-07:00	Small spiky stable layer	E
07:00-08:00	Breaking of inversion	B
08:00-13:00	Wave Thermal plumes	A
13:00-17:00	Cloud Thermal plumes	B
17:00-18:00	During sunset	C
18:00-20:00	Extreme stable condition	F
20:00-00:00	Stable layer	E

Table 4.5 Foggy day (18 December 2014)

Hours	SODAR Structure	Class
00:00-02:00	Stable layer	E
02:00-05:00	Neutral condition	D
05:00-08:00	Stable and foggy layer	E
08:00-11:00	Fog and unstable layer	C
11:00-15:00	Thermal Plumes	A
15:00-16:00	Moderate unstable	B
16:00-20:00	Stable layer	F
20:00-00:00	Stable layer	E

CHAPTER 5

DEVELOPMENT OF WAVELET-NEURO-FUZZY MODEL FOR THE PREDICATION OF VENTILATION COEFFICIENT

5.1. Introduction

Metropolitan cities world over are characterized by their economic development and big population, resulting in increased human activity that, in turn, can lead to high pollution levels. Consequently, the air quality in these cities is severely affected. The ventilation coefficient, which is the product of mixing depth and the average wind speed, is an atmospheric condition which gives an indication of the air quality and pollution potential, i.e., the ability of the atmosphere to dilute and disperse the pollutants over a region. The higher the coefficient, the more efficiently the atmosphere is able to dispose the pollutants and the air is better quality. On the other hand, low ventilation coefficients lead to poor dispersal of pollutants causing stagnation and poor air quality leading to possible pollution related hazards. The ventilation coefficient is a function of mixing depth and the average wind speed through the mixing layer. A fluctuation in the values of either/both these quantities causes a variation in the ventilation coefficient. These processes need to be modelled by making use of events that occurred in the past to predict.

There are many different methods of mathematical modelling, which have been developed to forecast long-term precipitation. In these methods, a statistical approach, such as time series modelling, is a conventional method that has been widely used. Statistical modelling has many advantages over mathematical models. But the shortcomings of the statistical approach include handling nonlinear characteristics of data because the statistical models are usually based on the linear correlations of the data can be expressed with a correlation coefficient. To overcome the shortcomings of the statistical methods, many other models that address the nonlinearity includes artificial neural network (ANN), fuzzy inference system (FIS), wavelets etc. ANN is a pattern matching technique that uses a pair of input and output sets. ANN has been generally applied to forecast stream flow, precipitation, and drought. FIS is data-driven model similar to ANN for representing linguistic fuzzy if-then rules that are difficult to formulate through a model with crisp parameters. In Fuzzy logic data was divided into training and testing phases. The model results were compared with measured data. The comparison depends on statistical characteristics, different error modes and contour map method. Hence the fuzzy model provides more accurate

and reliable results. Wavelet analysis is used for good times and frequency multi resolution and it can diagnose signal main frequency component, with local information of the time series. Wavelet transforms provide useful decompositions of the original time series, wavelet-transformed data improve the ability of forecasting model by capturing useful information on various resolution levels. Wavelet analysis is an effective tool than the Fourier transform in analyzing non-stationary time series. Several studies have been performed using wavelet transform to analyze time series.

The present study aims to develop a reliable model for predication the ventilation coefficient which, is the product of mixing depth and the average wind speed, over CSIR-NPL sites Delhi covering about 8-year (January, February, March of 2006 to 2014) period. In this present study, a conjunction model of wavelet-Neuro-fuzzy is introduced to predication the ventilation coefficient of Delhi.

5.2 Sample Site

The daily mean value of ventilation coefficient calculated at CSIR-NPL, New Delhi of the last 8 years (January, February, March) have been considered a sample site in the present study. Out of 650 samples from 2006 to 2014, 497 have been used to develop the prediction model for ventilation coefficient time series and 150 data have been used for the test model. First three data points are used as the input values.

5.3. Artificial Neural Network (ANN)

Artificial Neural Network (ANN) is commanding non-linear modelling approach. Which is based upon human brain functioning. It identifies and learns the correlated patterns between inputs values and objective values. It networks with nodes or neurons, which are interconnected to each other. A general three-layered neural network, consists of several elements nodes. These systems hold an input layer comprising of hubs speaking to diverse input variables, the hidden layer comprising of numerous concealed hubs and an output layer comprising of output variables.

A three layered FFNN (feed forward neural network) based on backpropogation has been selected. There are three input modes, three hidden nodes with tan sigmoid transfer function and one output node with the linear transfer function. So for predicting the output, past three inputs have to be estimated. The momentum and learning rate has kept to 0.9 and 0.1 and it trained for 1000 epochs.

5.4. Wavelet transform

Wavelet could be depicted as a pulse of short time with finite energy that integrates to zero. Wavelets are located both in time and space. The first step of wavelet transforms corresponds to mapping signal f to its wavelet coefficients. Using this process two components are received i.e. A smooth version called approximation and a second component that corresponds to the deviations or the details of the signal. A decomposition of the signal f into a low frequency part a_1 and a high frequency part d_1 at level 1 represented by $f=a_1 + d_1$. Similarity the same procedure is performed on a_1 in order to obtain a decomposition in the finer scales: $a_1 = a_2 + d_2$. Recursive decomposition for the low frequency parts follows the directions.

5.5. Adaptive Network Based Fuzzy Inference Systems (ANFIS)

The adaptive neuro-fuzzy interface system (ANFIS) methods is used worldwide, as an estimator. It is able to approximate real continuous function on a compact set to a degree of accuracy.

- Rules. The if-then rules have to be determined somehow. This is usually done by 'knowledge acquisition' from an expert. It is a time consuming process that is fraught with problems.
- Membership functions. A fuzzy set is fully determined by its membership function. This has to be determined. If it's gaussian then what are the parameters?

The ANFIS approach learns the rules and membership functions from data.

ANFIS is an *adaptive network*. An adaptive network is network of nodes and directional links. Associated with the network is a learning rule - for example back propagation. It's called adaptive because some, or all, of the nodes have parameters which affect the output of the node. These networks are learning a relationship between inputs and outputs.

Adaptive networks cover a number of different approaches, but for our purposes, we will investigate in some detail the method proposed by Jang known as ANFIS. The ANFIS architecture is shown below. The circular nodes represent nodes that are fixed, whereas the square nodes are nodes that have parameters to be learnt.

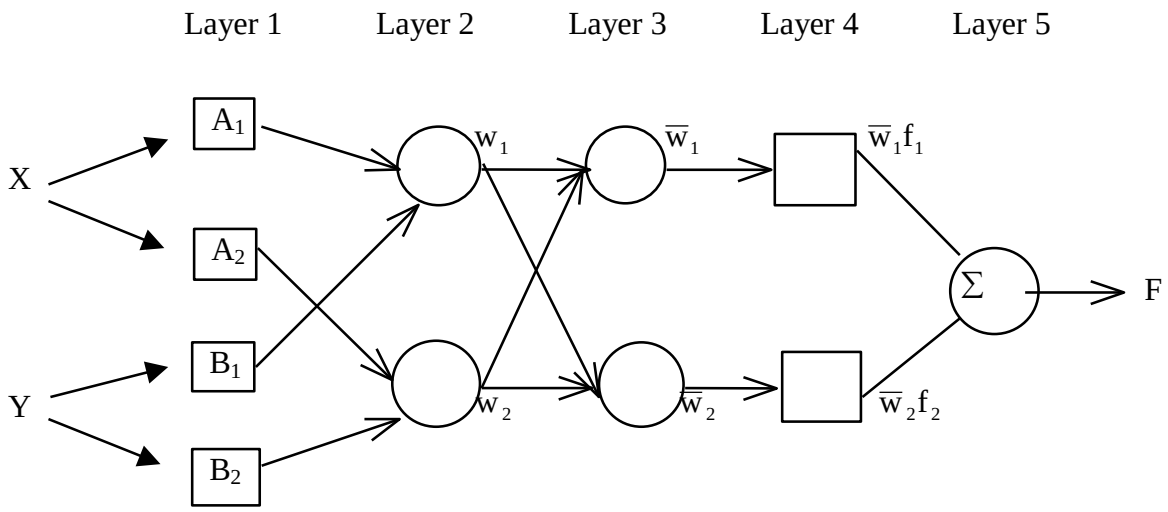

Figure 5.1. An ANFIS architecture for a two rule Sugeno system

A Two Rule Sugeno ANFIS has rules of the form:

$$If\ x\ is\ A_1\ and\ y\ is\ B_1 \quad THEN\ f_1 = p_1x + q_1y + r_1$$

$$If\ x\ is\ A_2\ and\ y\ is\ B_2 \quad THEN\ f_2 = p_2x + q_2y + r_2$$

For the training of the network, there is a forward pass and a backward pass. We now look at each layer in turn for the forward pass. The forward pass propagates the input vector through the network layer by layer. In the backward pass, the error is sent back through the network in a similar manner to backpropagation.

Layer 1

The output of each node is:

$$O_{1,i} = \mu_{A_i}(x) \qquad for\ i = 1,2$$

$$O_{1,i} = \mu_{B_{i-2}}(y) \qquad for\ i = 3,4$$

So, the $O_{1,i}(x)$ is essentially the membership grade for x and y.

The membership functions could be anything but for illustration purposes we will use the bell shaped function given by:

$$\mu_A(x) = \frac{1}{1 + \left| \frac{x - c_i}{a_i} \right|^{2b_i}}$$

where a_i, b_i, c_i are parameters to be learnt. These are the premise parameters.

Layer 2

Every node in this layer is fixed. This is where the t-norm is used to 'AND' the membership grades - for example the product:

$$O_{2,i} = w_i = \mu_{A_i}(x)\mu_{B_i}(y), \quad i = 1,2$$

Layer 3

Layer 3 contains fixed nodes which calculates the ratio of the firing strengths of the rules:

$$O_{3,i} = \overline{w}_i = \frac{w_i}{w_1 + w_2}$$

Layer 4

The nodes in this layer are adaptive and perform the consequences of the rules:

$$O_{4,i} = \overline{w}_i f_i = \overline{w}_i (p_i x + q_i y + r_i)$$

The parameters in this layer (p_i, q_i, r_i) are to be determined and are referred to as the consequent parameters.

Layer 5

There is a single node here that computes the overall output:

$$O_{5,i} = \sum_i \overline{w}_i f_i = \frac{\sum_i w_i f_i}{\sum_i w_i}$$

This then is how, typically, the input vector is fed through the network layer by layer. We now consider how the ANFIS learns the premise and consequent parameters for the membership functions and the rules.

There are a number of possible approaches, but we will discuss the hybrid learning algorithm proposed by Jang, Sun and Mizutani (Neuro-Fuzzy and Soft Computing, Prentice Hall, 1997) which uses a combination of Steepest Descent and Least Squares Estimation (LSE). This can get very complicated (!) so here I will provide a very high level description of how the algorithm operates.

It can be shown that for the network described if the premise parameters are fixed the output is linear in the consequent parameters.

We split the total parameter set into three:

S = set of total parameters

S_1 = set of premise (nonlinear) parameters

S_2 = set of consequent (linear) parameters

ANFIS uses a two pass learning algorithm:

- *Forward Pass. Here S_1 is unmodified anan S_2 is computed using a LSE algorithm.*
- *Backward Pass. Here S_2 is unmodified and S_1 is computed using a gradient descent algorithm such as back propagation.*

The hybrid learning algorithm uses a combination of steepest descent and least squares to adapt the parameters in the adaptive network.

5.6. Statistical Analysis of Ventilation Coefficient

Statistical properties are presented in table 5.1. The minimum value (115) and maximum value (5455) shows that the ventilation coefficient variation has a long range. It can be seen that the time series show high randomness and scattered distribution about the mean as the standard deviation (745) and variance are high. The training data considers the minimum and maximum inputs of data. This implies the trained neural network is not facing any difficulties in extrapolation.

Table 5.1 Statistical information of Ventilation coefficient of New Delhi

Data	No. of Sample	Mean	Standard Deviation	Variance	Maximum	Minimum	Median	Skewness	Kurtosis
Whole	650	1120	745	556645	5455	115	940	1.48	3.21
Training	500	1010	640	409425	3660	115	860	1.13	1.31
Testing	150	1480	935	875365	5455	160	1265	1.38	2.20

5.7. Neuro-Fuzzy-Wavelet coupled model

Before performing wavelet decomposition, three issues need to be resolved that are selection of mother wavelet, order of mother wavelet and the number of level decomposition. Attributes of the mother wavelet and the characteristics of the signal should be considered carefully, while choosing the appropriate wavelet. Daubechies are the most appropriate for treating random and spikes series. For these families of wavelet, the smoothness increases as the order of function increases and suitable wavelet and hence suitable higher order wavelet must be taken into account. In this work, wavelet of order 2 to 8 has been considered and it was observed that the decomposed series by wavelet of order 8 are giving the best results.

Figure 5.2 shows the signal approximation, A_3 and detailed parts D_1 to D_3. Approximation curves correspond to low frequency bands and represent the trends of the ventilation coefficient. Skewness is a measure of the symmetry of the data around the data mean and is zero for an ideal normal curve. Kurtosis refers to the degree of flatness.

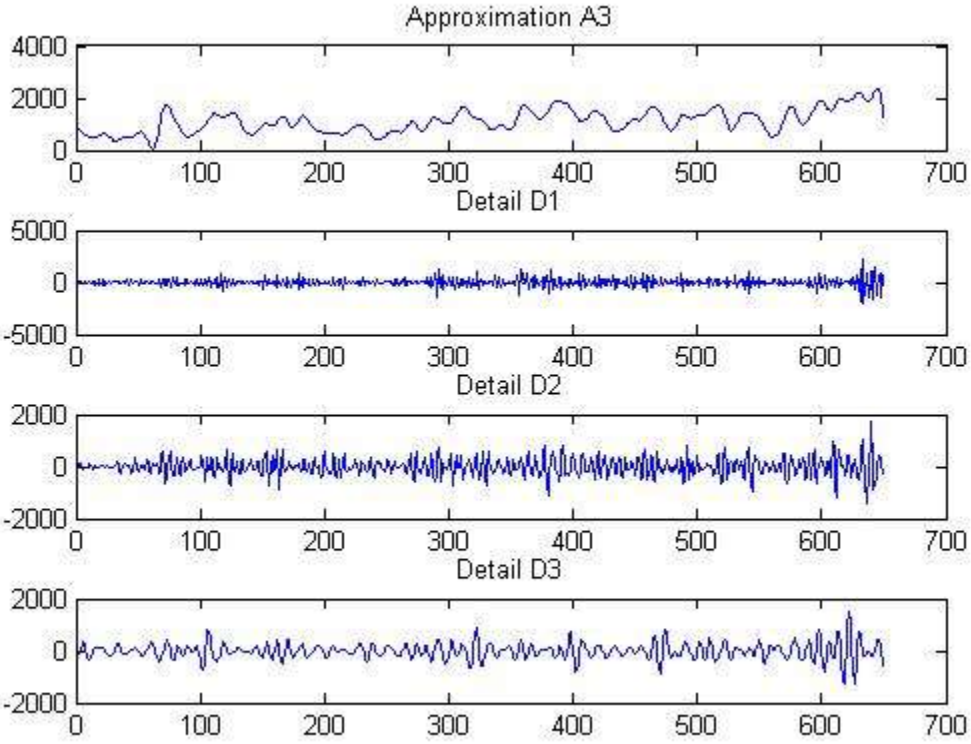

Figure 5.2 Detailed and Approximation coefficient using Daubechics (Db_8) wavelet

5.8 Experimental Results

The numerical experiments of predicting the future level of ventilation coefficient have been performed. The instrumental record data for training and testing have been collected from 2006 to 2014. 500 days data have been used for learning and the other part of 150 days for testing only. The results of learning and testing have been assessed on the basis of mean absolute error (MAE) and the predicted value.

The mean absolute value

$$MAE = \frac{1}{N}\left(\sum_{i=1}^{N}|d_i - y_i|\right)$$

where d denote the actual measurement, y is the predicted value and N is the number of days under predicted. The relative error is

$$\in = \frac{\|d - y\|}{\|d\|}$$

The neuro fuzzy wavelet predictor model has been developed and tested. The trained predicted output is obtained from the decomposed wavelet coefficients by simple summation represented by

$$S(n) = D_1 + D_2 + D_3 + A_3$$

Training and tested results by neuro-fuzzy-wavelet to predict 150 days ahead ventilation coefficient of New Delhi using Db_8 wavelet as follows:

MAE1= abs(sum(aactual)-sum(trained))/sum(aactual)

MAE1 = 0.0058

∈1= abs(sum(aactual)-sum(trained))/497

∈1 = 5.8792

MAE2= abs(sum(tested)-sum(arain15))/sum(arain15)

MAE2 = 0.0312

∈2= abs(sum(tested)-sum(arain15))/150

∈2 = 7.1881

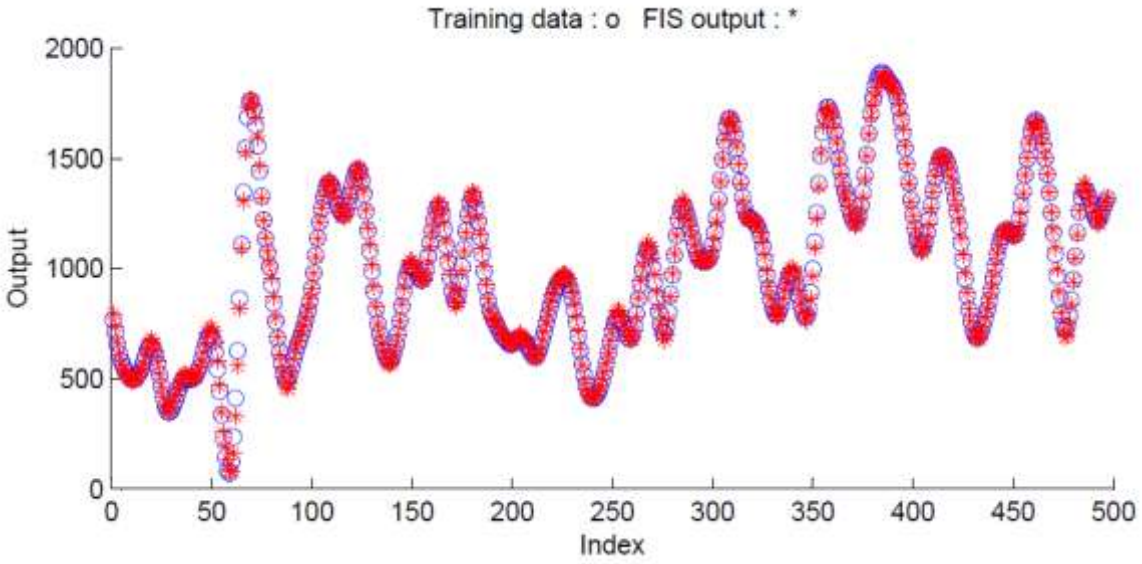

Figure 5.3 A_3 actual and trained results

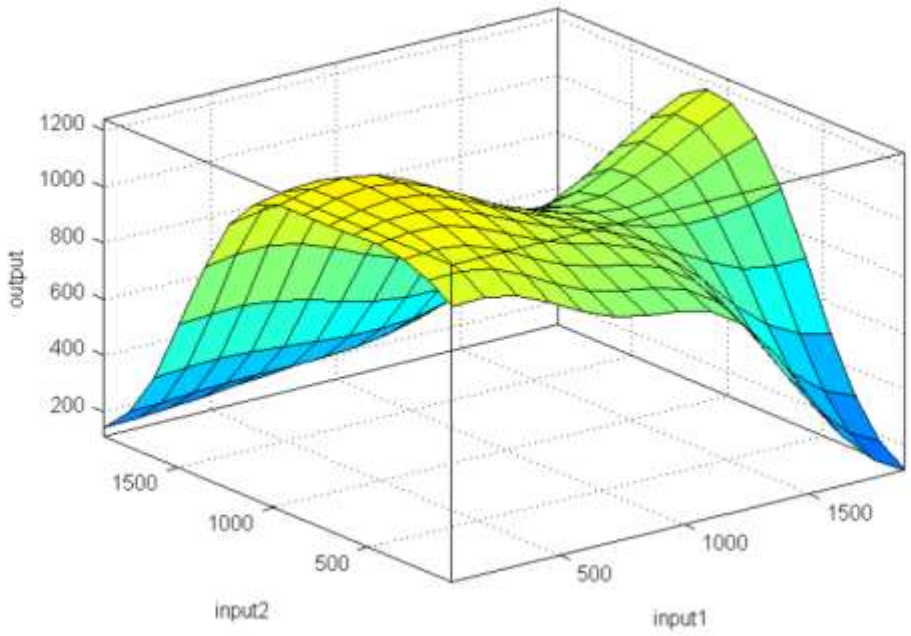

Figure 5.4 Surface view of A_3

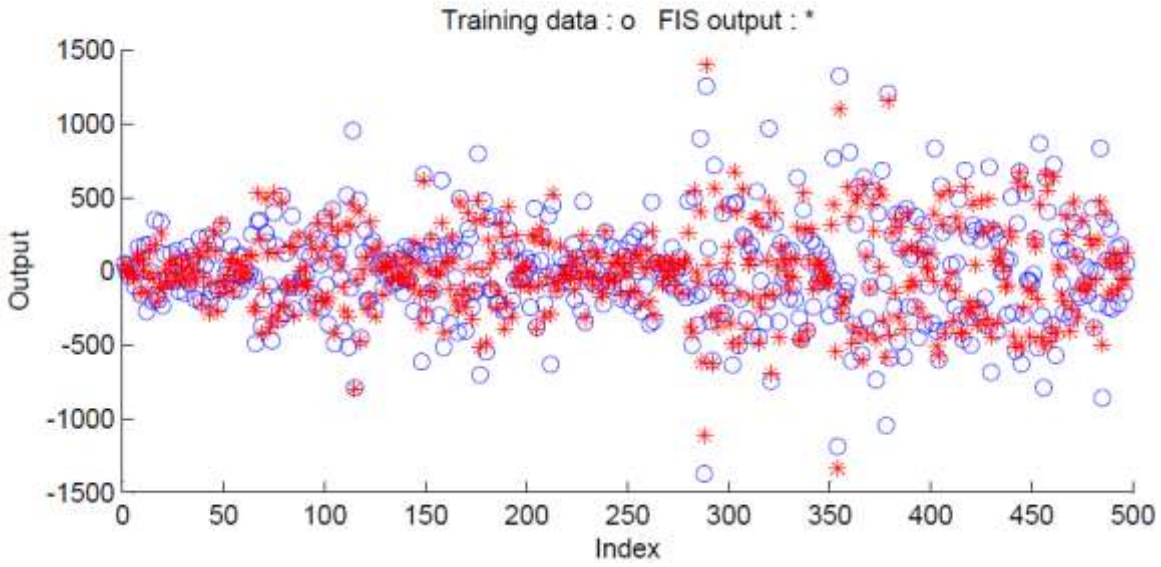

Figure 5.5 D_1 actual and trained results

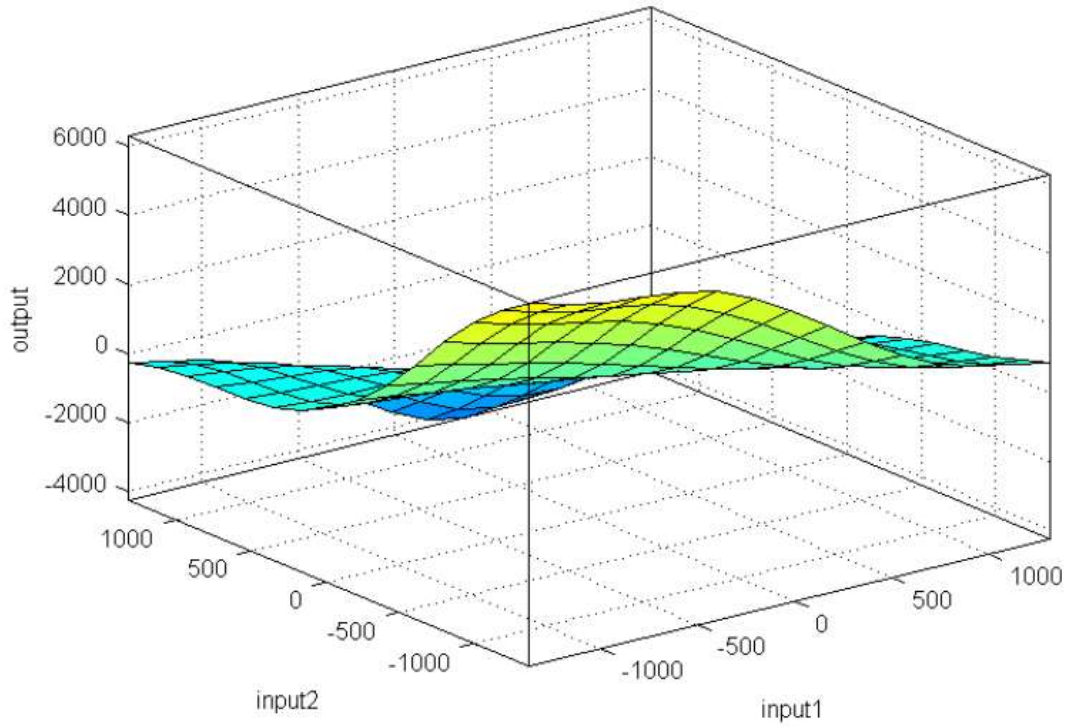

Figure 5.6 Surface view of D_1

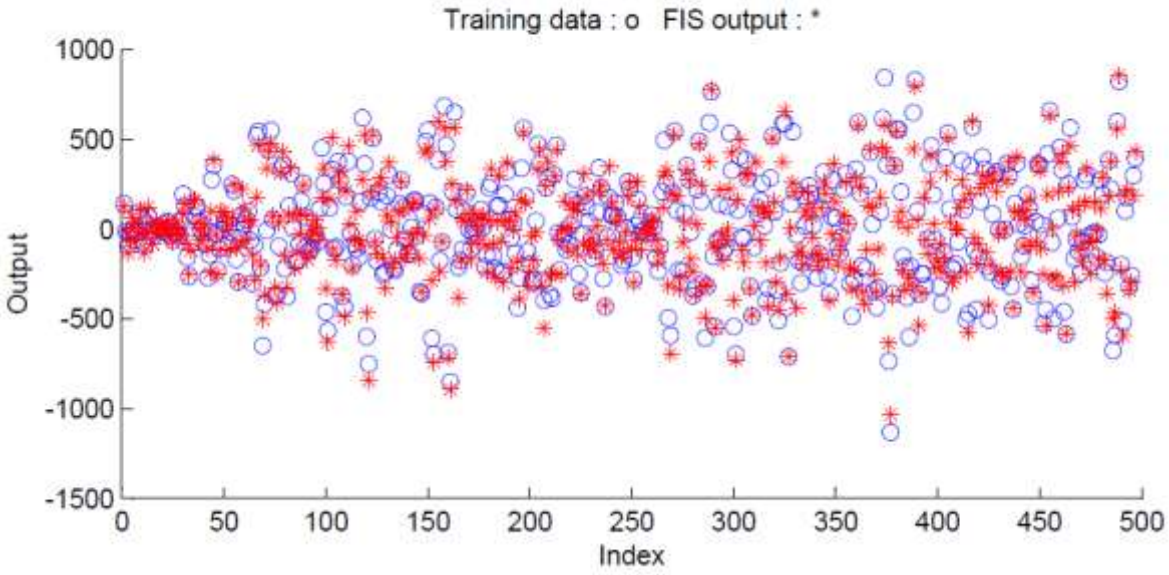

Figure 5.7 D_2 actual and trained results

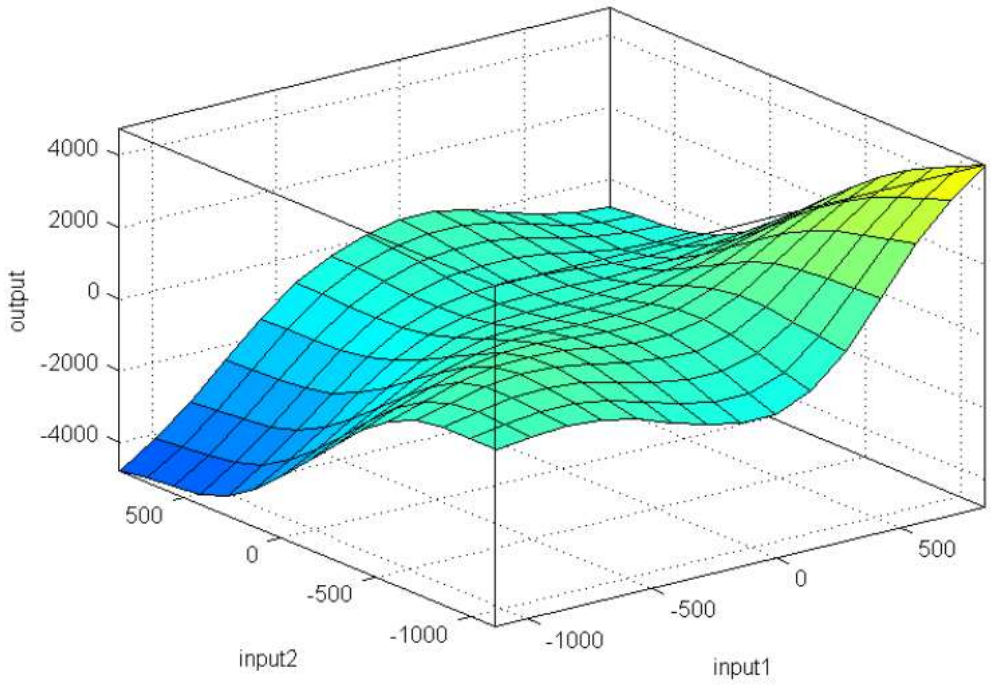

Figure 5.8 Surface view of D_2

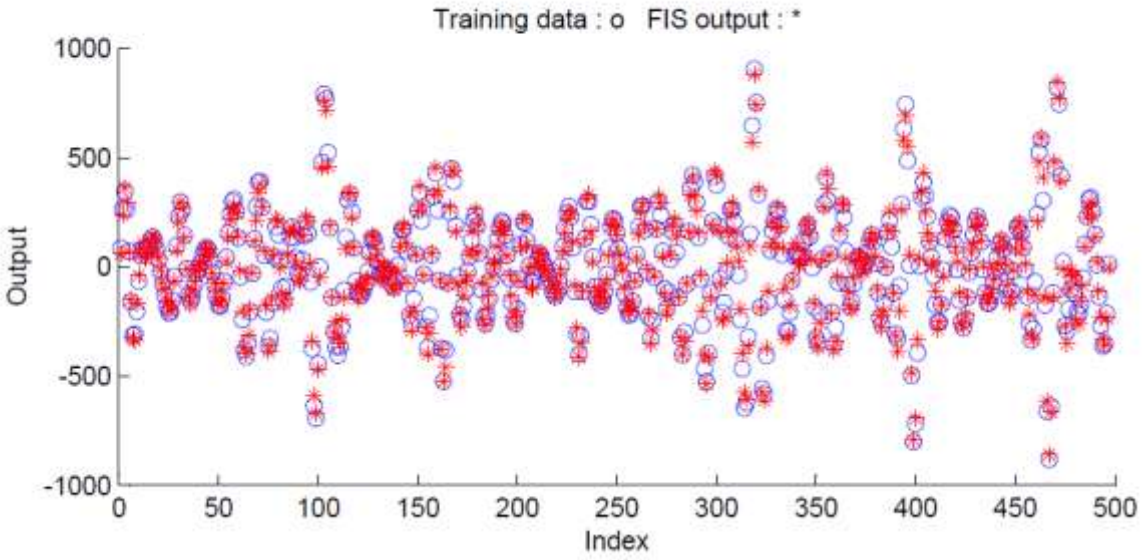

Figure 5.9 D_3 actual and trained results

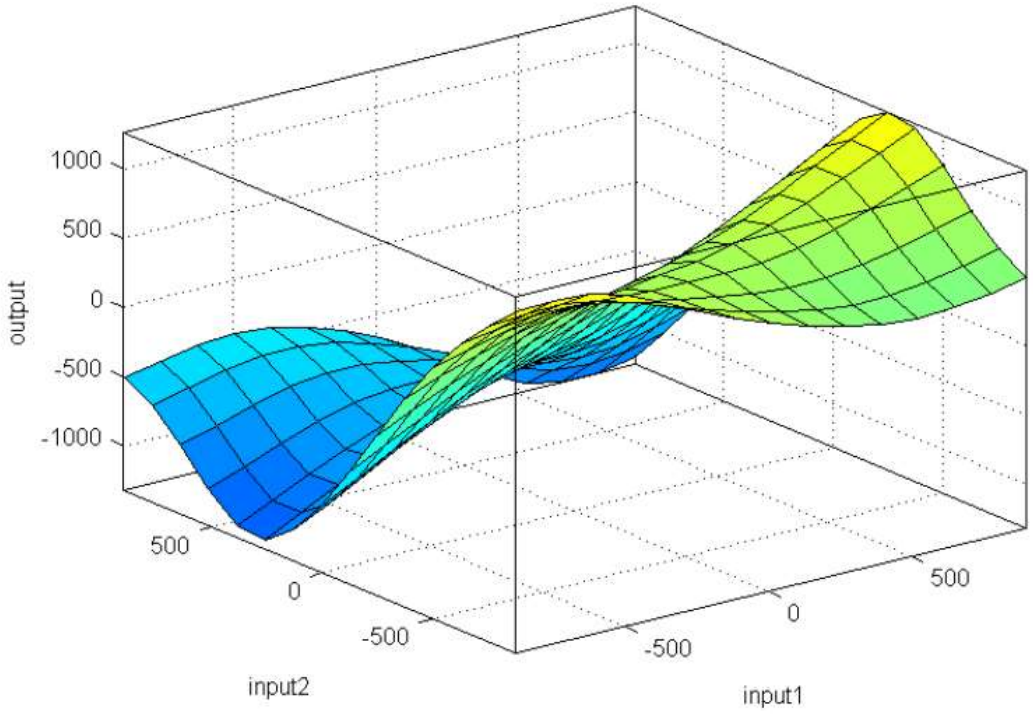

Figure 5.10 Surface view of D_3

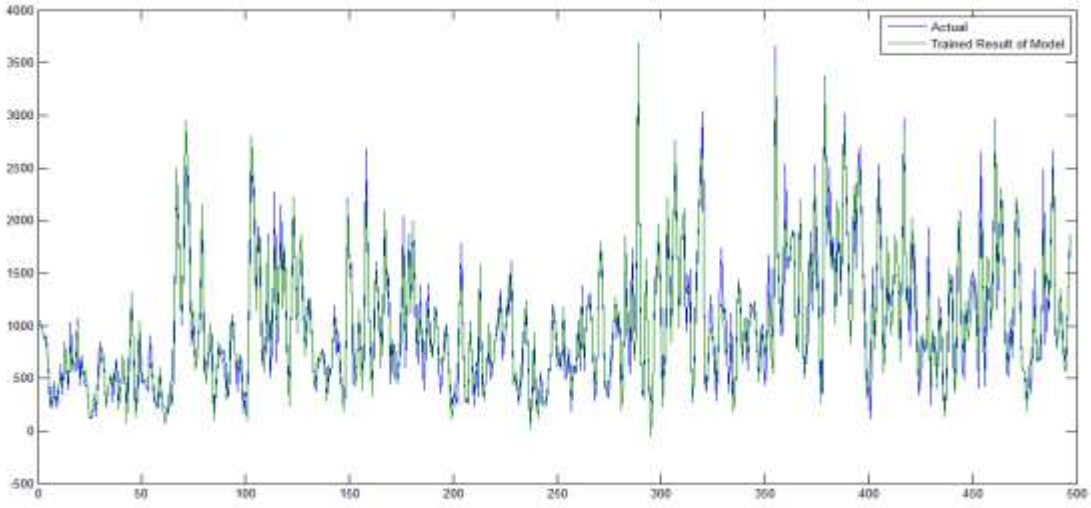

Figure 5.11 Actual output and predicated time series of average ventilation coefficient for training data using Neuro-Fuzzy-Wavelet

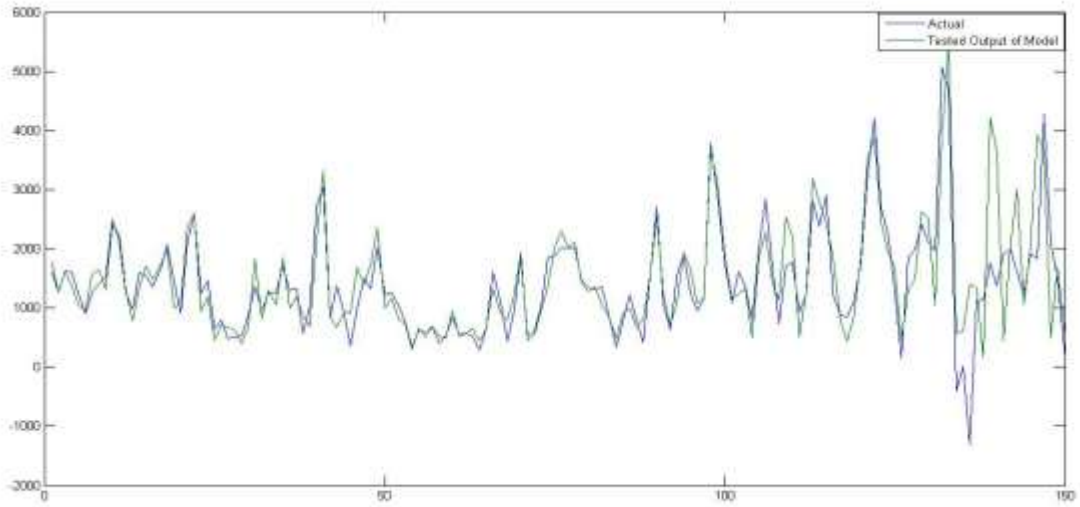

Figure 5.12 Actual output and predicated time series of average ventilation coefficient of testing data using Neuro-Fuzzy-Wavelet

CHAPTER 6
CONCLUSION

The SODAR is a useful remote sensing tool for investigations on characterization of boundary layer thermal structures. SODAR capabilities to provide on- line information on the atmospheric boundary layer structures can be used to derive air pollution concerned meteorological information on mixing height, inversion height, stability class, ventilation coefficient etc. which serve as useful input for stability classification using LabVIEW. An indigenously developed SODAR facility has been operating at CSIR-NPL, New Delhi in different weather condition and measured different types of echograms (like thundurm storm, foggy, cloudy *etc*.).

Comparative studies of the atmospheric boundary layer with respect to meteorological parameter have been performed. It is observed that ABL is positively correlated with temperature and wind speed whereas, negative correlation has been found with humidity. The average values of mixing height during the four seasons, winter, pre-monsoon, monsoon and post-monsoon have been found to be 555 ± 115 m, 650 ± 145 m, 535 ± 145 m, 365 ± 50 m respectively. The convective boundary layer height advances and decreases during the day time depending on the increase and decrease of surface temperature due to solar heating of the ground. From seasonal classification of stability class it is observed that, Class A and Class E was dominated in convection and nocturnal periods during all seasons, whereas class F was absent in winter and pre-monsoon seasons.

A reliable statistical model has also been developed for the predication the ventilation coefficient using a conjunction model of wavelet-Neuro-fuzzy model. The model so developed can be helpful in the predication of ventilation coefficient in different weather conditions. Further investigations focused on utilizing other soft computing techniques along with the development of Doppler SODAR and MiniSODAR should also be explored.

REFERENCE

[1] Bandopadhyay, L. K. and Chaulya, S. K. (2002). Application of acoustic sounding system for environmental study. *Minetech*, *23*(3), 37-46.

[2] Beyrich, F. (1997). Mixing height estimation from SODAR data—a critical discussion. *Atmospheric Environment*, *31*(23), 3941-3953.

[3] Choudhury, S., and Mitra, S. (2004). A connectionist approach to SODAR pattern classification. *Geoscience and Remote Sensing Letters, IEEE*, *1*(2), 42-46.

[4] Choudhury, S., and Mitra, S. (2006). Feature extraction and connectionist classification of SODAR echograms. *Geoscience and Remote Sensing Letters, IEEE*, *3*(1), 19-22.

[5] Gera, B.S. and Singal, S.P. (1990). Typical Boundary layer studies during monsoon period using SODAR. *Proceeding of the 5th international symposium on Acoustic Remote Sensing of the Atmosphere and Oceans, New Delhi Feb 6-9*, 390-394.

[6] Gera, B.S., Singal, S.P. and Ojha, V.K. (1990). SODAR studies of the boundary layer during a synoptic fog storm. *Proceeding of the 5th international symposium on Acoustic Remote Sensing of the Atmosphere and Oceans, New Delhi Feb 6-9*, 429-435.

[7] Gera, B. S., and Saxena, N. (1996). SODAR data— A useful input for dispersion modeling. *Atmospheric environment*, *30*(21), 3623-3631.

[8] Gera, N., Gupta, N.C., Mohanan, V. and Gera, B.S. (2013). SODAR studies of foggy atmospheric boundary layer over Delhi, *International Journal of Scientific and Engineering Research*, 4, 1634-1639.

[9] Gera, N., Gupta, N.C., Mohanan, V. and Gera, B.S. (2013). SODAR studies of air pollution meteorology over Delhi, *International Journal of Scientific and Engineering Research*, 4, 1805-1811.

[10] Ashrafi, K., and Hoshyaripour, G. A. (2010). A model to determine atmospheric stability and its correlation with CO concentration. *International Journal of Civil and Environmental Engineering*, *2*(2).

[11] Latha, R., and Murthy, B. S. (2011). Boundary layer signatures of consecutive thunderstorms as observed by Doppler SODAR over western India. *Atmospheric Research*, *99*(2), 230-240.

[12] Pasquill F., *Atmospheric Diffusion*, London, D. Van Nostrand Co. Ltd.1962.

[13] Roy, S., Adhikari, G. R., Renaldy, T. A., and Singh, T. N. (2011). Assessment of atmospheric and meteorological parameters for control of blasting dust at an Indian large surface coal mine. *Res. J. Environ. Earth Sci*, *3*(3), 234-248.

[14] Roy, S., Gupta, P., and Singh, T. N. (2012). Studies on Meteorological Parameters and Mixing Height in Gold Mining Area. *Resources and Environment*, *2*(5), 228-239.

[15] Singal, S. P., Gera, B. S., and Aggarwal, S. K. (1985). Studies of SODAR-observed dot echo structures. *Atmosphere-Ocean*, *23*(3), 304-312.

[16] Singal, S. P., Gera, B. S., and Saxena, N. (1997). SODAR: A tool to characterize hazardous situations in air pollution and communication. In *Acoustic remote sensing applications*, 325-384. Springer Berlin Heidelberg.

[17] Singal, S. P., Gera, B. S., and Pahwa, D. R. (1994). Application of SODAR to air pollution meteorology. *Remote Sensing*, *15*(2), 427-441.

[18] Singal, S. P. (1989). Acoustic sounding stability studies. *Encyclopedia of Environment Control Technology*, *2*, 1003-1061.

[19] Singal, S.P. (1989). SODAR studies of the convection boundary layer, *Journal of Scientific and Industrial Research* , 48, 84-91.

[20] SINGAL, S. (1989). Stable Boundary-Layer Studies Using Acoustic Sounding. *Journal of Scientific and Industrial Research*, *48*(8), 361-374.

[21] Singal, S. P. (1988). The Use of an Acoustic Sounder in Air-Quality Studies. *Journal of Scientific and Industrial Research*, *47*(9), 520-533.

[22] Singal, S. P. (1990). Current status of air quality related boundary layer meteorology studies using SODAR. *Acoustic Remote Sensing*, 453-476.

[23] Singal, S. P., Gera, B. S., and Aggarwal, S. K. (1983, August). Studies of the boundary layer at Delhi using SODAR. In *Proc. 2nd Symp. ISARS, Rome*, 23-28.

[24] Singal, S. P., Gera, B. S., and Aggarwal, S. K. (1984). Nowcasting by Acoustic Remote-Sensing-Experiences with the Systems Established at the National-Physical-Laboratory, New-Delhi. *Journal of Scientific and Industrial Research*, *43*(9), 469-488.

[25] Thomas, P. (1986). Stability classification by acoustic remote sensing. *Atmospheric Research*, *20*(2), 165-172.

[26] Ramachandran, S., Kedia, S., and Srivastava, R. (2012). Aerosol optical depth trends over different regions of India. *Atmospheric Environment*, *49*, 338-347.

[27] Aggarwal, S. K., Singal, S. P., and Srivastava, S. K. (1980). SODAR studies of gravity waves in the planetary boundary layer at Delhi. *Mausam*, *31*, 373.

[28] Parmar, K. S., and Bhardwaj, R. (2015). River Water Prediction Modeling Using Neural Networks, Fuzzy and Wavelet Coupled Model. *Water Resources Management*, *29*(1), 17-33.

[29] Manju, N., Balakrishnan, R., and Mani, N. (2002). Assimilative capacity and pollutant dispersion studies for the industrial zone of Manali. *Atmospheric Environment*, *36*(21), 3461-3471.

[30] Lu, C., Deng, Q. H., Liu, W. W., Huang, B. L., and Shi, L. Z. (2012). Characteristics of ventilation coefficient and its impact on urban air pollution. *Journal of Central South University*, *19*, 615-622.

[31] Mahalakshmi, D. V., Badarinath, K. V. S., and Naidu, C. V. (2011). Influence of boundary layer dynamics on pollutant concentrations over urban region- A study using ground based measurements. *Indian Journal of Radio and Space Physics*, *40*(3), 147-152.

PUBLICATIONS

[1] Kumar, N., Agarwal, R., Soni, K., and Singh, G. (2015). Development on LabVIEW based program for the Classification of Stability Class in SODAR Observations. *National symposium on Acoustics "Acoustics for Ocean Environment" 7-9 October 2015*. (Accepted)

[2] Kumar, N., Soni, K., Agarwal, R., Garg, N., Saha, D., Singh, M. and Singh, G. Seasonal variability of stability class and its dependence on meteorological parameters. *International Journal of Remote Sensing.* (Communicated)